universität wien

MASTERARBEIT | MASTER'S THESIS

Titel | Title

The activation of mtUPR in WNT activated human cells and mice brains

verfasst von | submitted by

Veronika Fleischhart

angestrebter akademischer Grad | in partial fulfilment of the requirements for the degree of

Master of Science (MSc)

Wien | Vienna, 2024

Studienkennzahl lt. Studienblatt | Degree programme code as it appears on the student record sheet:	UA 066 834
Studienrichtung lt. Studienblatt | Degree programme as it appears on the student record sheet:	Masterstudium Molekulare Biologie
Betreut von | Supervisor:	Assoz. Prof. Dr. Florian Raible

Declaration of Independence

I declare that this master's thesis was written by myself, that I have not used any aids other than those mentioned above, and that I have not used any other unauthorised help.
I certify that I have not submitted this master's thesis as an examination paper in any form, either in Austria or abroad (to an assessor for review).
Furthermore, I certify that the copies I have submitted (printed and electronic) are identical.

Date: Signature:

....

Acknowledgements

I want to express my gratitude to everyone who helped, understood, and taught me on the way. This significant step of a master's thesis would not have been possible without my colleagues and now also close friends in the lab. Angie Torres was my supervisor and taught me with much patience. Rodrigo Mira always helped if problems came up or questions arose. Cristina Pinto was teaching me how to handle worms. I was also allowed to meet more great people in the lab who became my friends. Therefore, a big thank you to Angelica, Damaris, Vania, Karla, and Mariajose for helping me with the lab work.
Further, I want to thank Professor Nibaldo Inestrosa for caring about the financial aspect, developing new ideas, and providing excellent knowledge.
I received help finding coding mistakes from Michael Übl for the bioinformatic analysis code.
I must thank all my friends at home who stayed in contact with me and celebrated achievements with me online.
Last but not least, I need to express my great thankfulness to my parents, without whom this stay would not have been possible. Their financial support throughout my whole study program and all their advice helped me to come this far.

Thank you all for your support.

Abstract

Alzheimer's Disease is an ageing-associated disease and is becoming more prevalent in aged populations. The main characterisations are tau tangles and Aβ plagues. WNT and mitochondrial unfolded protein response negatively influence both structures. In the early 2000s, researchers found the influence of the WNT signalling pathway on Alzheimer's disease. Recently, however, a link to mitochondrial unfolded protein response has also been investigated. Activating one of the two signalling pathways reduces the toxic aggregates and can improve symptoms. This study aims to investigate the connection between these two signalling pathways in mammals to understand the disease and its underlying changes better. Lithium chloride was used to simulate the activation of the WNT signalling pathway in human cells and mouse brains. Proteins from both pathways were analysed using Western blot analysis. These experiments proved the activation of the WNT pathway and investigated the activation of the mitochondrial unfolded protein response. In human cells, results show a tendency indicating that WNT activation increases the mitochondrial unfolded protein response. In the brains of mice, WNT activation leads to a significant increase in mtUPR proteins in the hippocampus. Due to the association of tau and amyloid β with both signalling pathways, understanding the interaction between them can help to find future treatment options.

Zusammenfassung

Alzheimer gehört zu den Alterungserkrankungen und die Zahl der Betroffenen steigt durch die wachsende Alterung der Bevölkerung. Die beiden Hauptmerkmale sind Tau Tangles und Aβ Plaques. Beide Proteine werden von WNT und mtUPR negativ beeinflusst. Der Zusammenhang des WNT-Signalwegs und der Alzheim-Ererkrankung wurde schon zu Beginn der 2000er gefunden. Kürzlich jedoch wurde auch eine Verbindung zu mtUPR näher beleuchtet. Durch die Aktivierung von einem der beiden Signalwege verringern sich die toxischen Aggregate beider Proteine und es kommt zu einer Verbesserung der Symptome. In dieser Studie wird die Verbindung dieser beiden Signalwege in Säugetieren erforscht, um ein besseres Verständnis für die Erkrankung und die zugrunde liegenden Prozesse zu bekommen. Dafür wurde mit Hilfe von Lithiumchlorid die Aktivierung des WNT-Signalwegs in menschlichen Zellen und Gehirnen von Mäusen simuliert. Die Proteine beider Signalwege wurden durch Western Blots analysiert. Dadurch wird die Aktivierung vom WNT-Signalweg überprüft und die Veränderung des mtUPR-Signalweges untersucht. Die Ergebnisse in humanen Zellen zeigten eine Tendenz, die darauf hindeutet, dass die Aktivierung von WNT die Menge an mtUPR Proteinen erhöht. In den Gehirnen von Mäusen führt die Aktivierung von WNT zu einem signifikanten Anstieg an mtUPR Proteinen. Durch den Zusammenhang von Tau und amyloid β mit beiden Signalwegen, kann das Verständnis der Interaktion dabei helfen zukünftige Behandlungsmöglichkeiten zu finden.

Abbreviation

AD	Alzheimer‘s Disease
AKT	Protein Kinase B
AMPA	α-amino-3-hydroxy-5-methyl-4-isoxazole propionic acid
APC	Adenomatous polyposis coli
APP	Amyloid precursor protein
ATF	Activating transcription factor
ATFS-1	Stress-activated transcription factor
AU	Arbitrary unit
Aβ	Amyloid beta
BACE	β-secretase
Bp	Basepairs
CBP	cAMP-response-element-binding protein (CREB)-binding protein
CK1	Casein kinase 1
ClpP	Caseinolytic mitochondrial matrix peptidase
Dkk1	Dickkopf-related protein 1
DVE-1	Homeobox protein DVE-1 or Defective proventriculus homolog protein
DVL	Dishevelled
eIF2α	Eukaryotic translation initiation factor 2 alpha
erUPR	Endoplasmatic reticulum unfolded protein response
FAD	Familiar Alzheimer’s disease
FBS	Fetal bovine serum
FZD	Frizzled
GSK3	Glycogen Synthase Kinase 3
GSK3pY216	Glycogen Synthase Kinase 3β phosphorylated on tyrosine 216
Hsp	Heat shock protein
ISR	Integrated stress response
LEF	Lymphoid enhancer factor
Lonp	LON protease
LRP	Low-density lipoprotein receptor-related protein
LTP	Long-term potentiation
MAP	Microtubule-associated protein
mt	Mitochondrial
MTS	Mitochondrial targeting sequence
mtUPR	Mitochondrial unfolded protein response
NLS	Nuclear location sequence
NMDA	N-methyl-D-aspartate
OMA1	m-AAA protease 1
ORF	Open reading frame
pGSK3	Glycogen Synthase Kinase 3β phosphorylated on serin 9
PI3K	Phosphatidylinositol 3-kinase
PSD95	Postsynaptic density protein 95
RNA	ribonucleic acid
SAD	Sporadic Alzheimer’s disease
TCF	T-cell factor
TOM	Translocase of the outer membrane
TIM	Translocase of the inner membrane
UBL-5	Ubiquitin-like protein 5
WNT/PCP	WNT/Planar Cell Polarity
VDAC	Voltage-dependent anion channel

Key terms: Alzheimer's Disease, mtUPR, WNT, SHSY5Y cell line, C57BL/6J mouse

Table of content

Declaration of Independence 1
Acknowledgements 2
Abstract 3
Zusammenfassung 4
Abbreviation 5
1 Introduction 7
1.1 Molecular cause of Alzheimer's Disease 7
1.2 Molecular aspects of WNT and its relation to AD 9
1.3 Molecular aspects and role of Mitochondrial unfolded protein response 12
1.3.1 Defining mitochondrial unfolded protein response 13
1.3.2 The activation of the Mitochondrial unfolded protein response and its consequences 13
1.3.3 The role of mtUPR in Alzheimer's disease 15
1.3.4 Recent findings on the relation of WNT signalling and mtUPR 17
1.4 Aim of thesis 17
2 Results 18
2.1 Analysing the Promotor of mtUPR genes to investigate a possible WNT regulation 18
2.2 WNT activation in SHSY5Y cells with different Lithium chloride concentrations 19
2.3 Attempt to differentiate SHSY5Y cells for a stronger neuronal phenotype 22
2.4 Investigation of mtUPR protein levels in WNT active cells 24
2.5 Testing Immunofluorescence analysis in cells to follow the translocation of ATF5 and β-catenin 28
2.6 mtUPR protein levels in mice cortex and hippocampus after LiCl treatment 29
3 Discussion 33
4 Methods 37
4.1 Bioinformatic promotor analysis 37
4.2 Cell culture 37
4.2.1 SHSY5Y cells 37
4.3 Animals and experimental procedures 38
4.4 Western Blot 38
4.5 Statistics 40
5 Bibliography 41
6 List of Figures 48
7 List of tables 50
8 Additional information 51
8.1 Example pictures of Immunohistochemistry experiments 51
8.2 Method: Immunofluorescence 51
8.3 Materials 52
8.3.1 Western Blot 53
8.3.2 Cell culture 54
8.3.3 Mice treatments 54
8.3.4 Immunofluorescence 54
8.3.5 Antibodies 54
8.4 Python source code for Immunofluorescence analysis 57
8.4.1 Creation of merged images 57
8.4.2 Analysis of intensity in and out of the nucleus 58

1 Introduction

1.1 Molecular cause of Alzheimer's Disease

Alzheimer's disease (AD) is the most common type of dementia and an ageing-related disease, which will lead to an increase in AD patients in the future due to the rising life expectancy of humans [1]. Statistical evaluations predict that the cases of AD will double in the next 25 years. Figure 1 shows the percentage of dementia and Alzheimer's Disease cases per population in Austria compared to Chile, Europe and worldwide. In 2018, 146.801 Austrians over 30 years old received an AD diagnosis [2]. 9,1 million patients over 30 years suffered in Europe from AD in 2018, and in 2019, the OECD reported 50 million cases over 40 years of age worldwide [3]. In Chile, approximately 180.000 people suffered from some form of dementia in 2009 [4]. Most patients receive the diagnosis when reaching 65 years or more [2], [4]. Predictions for 2050 show an increase of up to 290.499 patients in Austria, 626.000 in Chile, 16,3 million cases in Europe and 139 million worldwide [2], [4]. Statistical evaluation showed that approximately 2/3 of dementia diagnoses are Alzheimer's disease [2], [5].

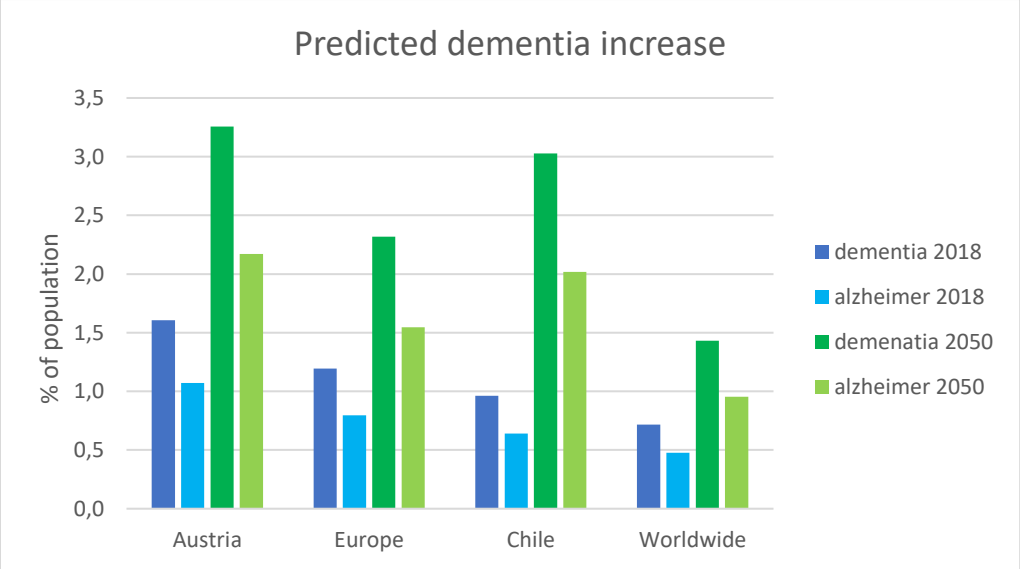

Figure 1: Dementia and Alzheimer's cases today and in the future
The graph shows dementia and Alzheimer's cases in percentages related to the region's population.
The population prediction comes from the website populationpyramid.net [6]. It displays the increase in AD cases predicted for 2050.

AD starts with spatial memory loss, leading to patients becoming disoriented in familiar environments, which can result in an increased risk of patients injuring themselves. As it continues, the personalities of patients change due to troubles during daily life chores, which burden their mental health. Patients can also suffer from losing the ability to recognise their loved ones and might lose the ability to connect everyday events with their reality. Today, patients are diagnosed due to an irreversible cognitive decline together with the aggregation of tau and amyloid β (Aβ) peptide into neurofibrillary tangles and senile plagues [1].

In AD, there are two forms, familial Alzheimer's disease (FAD) and sporadic Alzheimer's disease (SAD). These two differ in their time of onset. While FAD occurs mainly in people under 60 years, SAD occurs in older patients. However, 95% of all AD cases are SAD, of which the exact cause is unknown today [7]. The cause of FAD, the inheritable form of AD, is autosomal-dominant mutations in proteins like Amyloid precursor protein (APP),

presenilin 1 or presenilin 2 [8]. APP is a transmembrane protein which plays a significant role in synaptic processes [9]. Both presenilins participate in protein complex formation to regulate the cleavage of APP, leading to senile plaques [10].
Figure 2 shows the two APP processing paths. The amyloidogenic pathway leads to the pathogenic product, and the harmless product comes from the non-amyloidogenic pathway [11]. During the non-amyloidogenic pathway, the enzyme α-secretase cuts between the 15 and 17 amino acids of APP, and the enzyme γ-secretase cuts at the C-Terminus. The α-secretase inhibits the formation of the toxic product by cutting through the area needed for the pathogenic Aβ [12]. For the amyloidogenic way, the enzyme β-secretase, also called BACE, cuts at the N-terminus instead of the α-secretase, forming the amyloid beta peptide. The enzyme γ-secretase is not always cutting exactly. Therefore, different types of products like Aβ40 and Aβ42 exist. In healthy individuals, the production of Aβ40 is greater than Aβ42, which is the main component of plaques [13]. Studies showed that mutations within the catalytic subunit of γ-secretase, presenilin 1, and presenilin 2 lead to more Aβ42 and mutations in the APP protein itself [13].

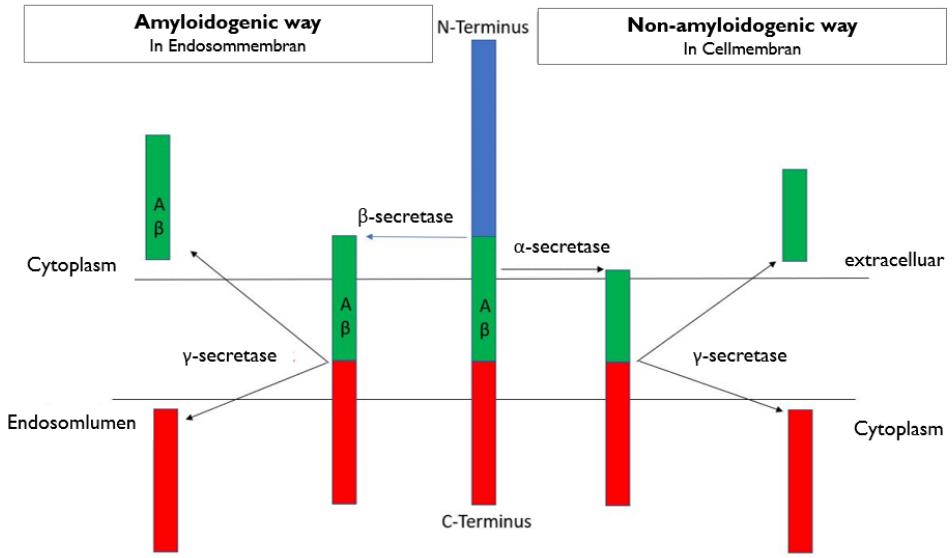

Figure 2: The two pathways of APP processing forming the toxic and non-toxic product
The figure shows the processing of APP by α, β and γ-secretase. It displays the non-amyloidogenic way on the right side and the amyloidogenic one on the left, leading to the harmful Aβ.
Inspiration comes from the figures from Yun-wu Zhang et al. l.[14] and Jing Zaho et al. l.[11].

Two hypotheses exist to explain the primary cause of cognitive impairment in AD: the Aβ and tau hypotheses. Aβ peptides can accumulate from oligomers to fibrils and form senile plaques in the end [7]. Thereby, senile plaques are the least synaptotoxic aggregation of Aβ [15]. Research showed that a change in the ratio of Aβ isoforms can lead to tau hyperphosphorylation and, therefore, to cognitive decline, indicating that Aβ could be the primary cause [7].
However, different studies show hyperphosphorylated tau without Aβ aggregation [7]. Tau can form neurofibrillary tangles when posttranslational hyperphosphorylated, impairing neurons' transport [7].
These findings support both hypotheses trying to explain which protein is the primary cause of AD [7].

Tau is an essential microtubule-associated protein (MAP) which plays an important role in normal brain functioning [16]. Tau interacts with microtubules in neuronal axons, helps with their assembly, and stabilises them. However, it also plays a role in axonal transport by interfering with the binding of motor proteins [17]. Many posttranslational

modifications like acetylation or ubiquitylation regulate tau, but phosphorylation is the most important. It is highly regulated since phosphorylation reduces the positive charge of tau. Thus, tau phosphorylation reduces the binding to microtubules, destabilising them [17]. Kinases and phosphatases perform this regulation. One essential kinase is Glycogen Synthase Kinase 3 (GSK3), which has two isoforms GSK3α and GSK3β. GSK3β plays a major role in WNT signalling, while GSK3α only takes part in WNT signalling when GSK3β is impaired [18]. Research shows that an increase in GSK3β activity correlates with an increase in tauopathies, and an increase of GSK3β within tauopathies results in stronger neurodegeneration [17]. Tau hyperphosphorylation occurs during development and AD.
In early development, only the shortest isoform of tau is present and hyperphosphorylated. This process degrades unused neurons and axonal paths since neuronal development is strongly interconnected with degeneration [19]. AD increases the hyperphosphorylation of tau and affects longer isoforms, leading to neurodegeneration of needed neurons [19]. It also leads to paired helical filaments forming, which can interact and accumulate from straight filaments to neurofibrillary tangles [20]. Hyperphosphorylated tau can function as a centre where normal tau can bind, reducing the amount of tau that functions normally [21]. Hyperphosphorylated tau can also interact with other MAPs by binding them into the formed tangles [14]. The formation of oligomers and neurofibrillary tangles and the misfunctioning of MAPS disturb the normal function of neurons by impairing their transport machinery. However, functioning transport is important for neurons because the cell soma produces many molecules that need the transport machinery to reach the synapse, and the synapse produces signalling molecules needed in the cell soma. Therefore, failure of the neuronal transport can result in neurodegeneration and dementia-like symptoms [16], [22].
An important area affected by these changes is the hippocampus, which is part of the central nervous system. Adult neurogenesis occurs in the hippocampus and the cerebral cortex. Essential functions of the hippocampus are spatial learning and memory formation. The dysfunction of this area also explains the previously mentioned AD symptoms [23]. Researchers have shown that Aβ peptides can lead to memory loss and learning deficits before neurodegeneration. The reason for this is the blocking of long-term potentiation (LTP) [24]. Long-term potentiation means increased use of synapses, which leads to strengthening memory formation and increased signal transmission [25].

1.2 Molecular aspects of WNT and its relation to AD

As mentioned above, the WNT-related kinase GSK3β plays a role in the hyperphosphorylation of tau and leads to tauopathies. It also increases Aβ when active, leading to senile plagues. Together, both proteins can form a vicious cycle with GSK3β [26], [27], [28]. An imbalance between the canonical and non-canonical WNT pathways impairs neurons during AD [29].
WNT signalling is a form of cell-to-cell communication that can cause disorders and abnormalities due to overexpression or deficiency. The activation of the WNT pathway results in various functions, defined by 19 small cysteine-rich proteins called ligands, 10 receptors, and alternative receptors [30], [31]. These factors also determine the activation of the canonical or non-canonical pathways [32]. WNT signalling plays a role in metabolic and cellular functions like movement, proliferation, and differentiation [30]. It plays a significant role in the central nervous system, especially in synapses and neurogenesis. WNT influences neurogenesis in adult brains, synaptogenesis during development, and spine formation. WNT ligands also affect the active region of synapses, including the presynaptic receptors, neurotransmission sites, and postsynaptic assembly. WNT ligands inducing the canonical

pathway, also called WNT/β-catenin, regulate the presynaptic function, and non-canonical WNT, WNT/Planar Cell Polarity (WNT/PCP) and WNT/Ca^{2+} play a role in the postsynaptic assembly and function [33]. All signalling cascades regarding WNT count either to the canonical or the noncanonical pathway [30], [34].

Figure 3 shows the canonical WNT pathway in the absence and presence of WNT ligands. Frizzled (FZD), a seven-pass transmembrane receptor protein in the cell membrane of other WNT-responsive cells, recognises WNT ligands. Frizzled receptors interact with a low-density lipoprotein receptor-related protein (LRP). Only if both proteins associate the binding of a WNT ligand occurs and initiates a cascade in the cell. In the absence of WNT ligands, the destruction complex containing scaffolding proteins such as Axin, adenomatous polyposis coli (APC), the kinases GSK-3β and casein kinase 1 (CK1) marks β-catenin for degradation. GSK3β and casein kinase 1 phosphorylated β-catenin, which leads to ubiquitination by E3-ubiquitin ligase β-TrCP, leading to proteasome degradation.
When WNT binds to the receptors, the lipoprotein receptor-related protein is phosphorylated and attracts Dishevelled (DVL) proteins. That leads to the dissociation of the destruction complex and the stabilisation of β-catenin. Now, β-catenin can translocate to the nucleus and induce transcription, where it interacts with the T-cell factor (TCF) and lymphoid enhancer factor (LEF) [34], [37], [38], as seen in Figure 3. TCFs in the nucleus function as a transcriptional switch by recruiting transcriptional suppressors. If β-catenin replaces these suppressors, other transcriptional co-activators like p300 and cAMP-response-element-binding protein (CREB)-binding protein (CBP) can bind and induce gene transcription.
Therefore, GSK3β inhibition induces β-catenin translocation and simulates the activation of the WNT pathway. One GSK3β inhibitor is Lithium, which can inhibit GSK3β directly or indirectly by either competing with magnesium and leading to an allosteric change similar to WNT binding or by activating the phosphatidylinositol 3-kinase (PI3K) Akt signalling pathway [35]. Akt, also called Protein kinase B, is a serine/threonine-specific protein kinase which can lead to phosphorylation of GSK3β [36]. Figure 4 displays both pathways of GSK3β inhibition by lithium chloride (LiCl).

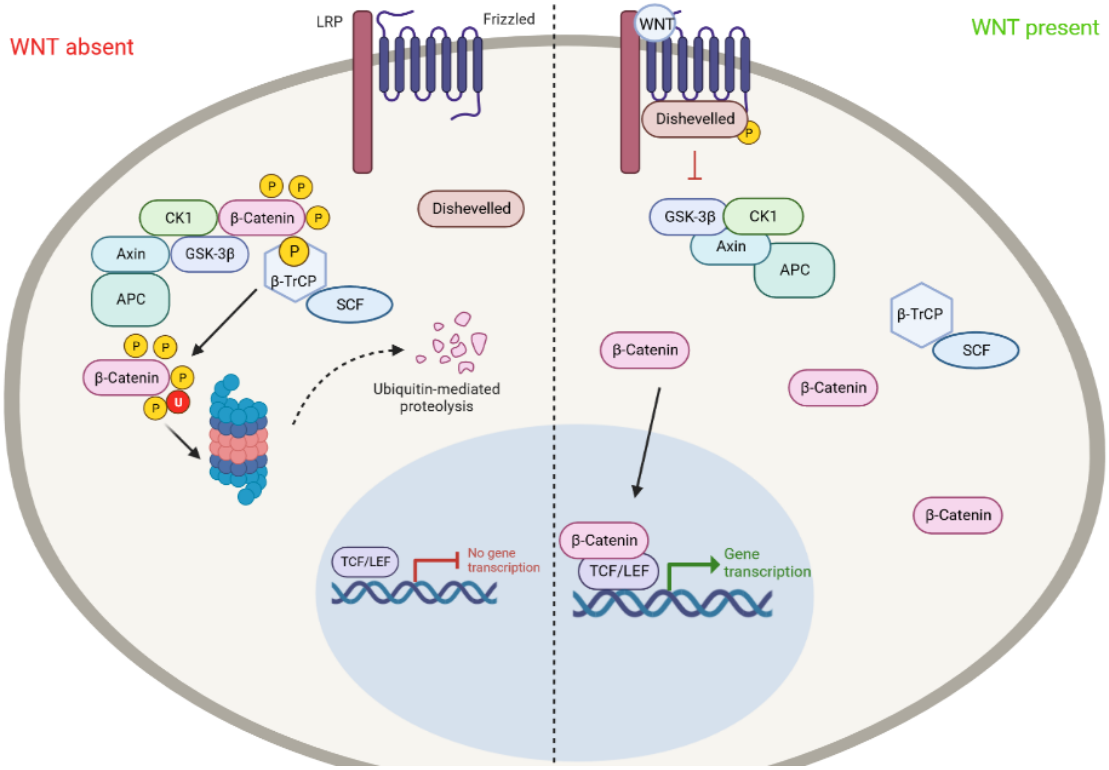

Figure 3: The canonical WNT pathway and its key players

This figure shows the different players in the canonical WNT pathway in the absence and presence of WNT ligands. It is inspired by figures seen in papers [34], [37], [38] and created using biorender. On the left side is the pathway displayed in the absence of WNT, where the destruction of complex phosphorylated β-catenin leads to proteasome degradation after ubiquitination by β-TrCP. On the right side, the WNT ligand binds to Frizzled and LRP, inhibiting the destruction complex, the translocation of β-catenin, and the increase in gene transcription.

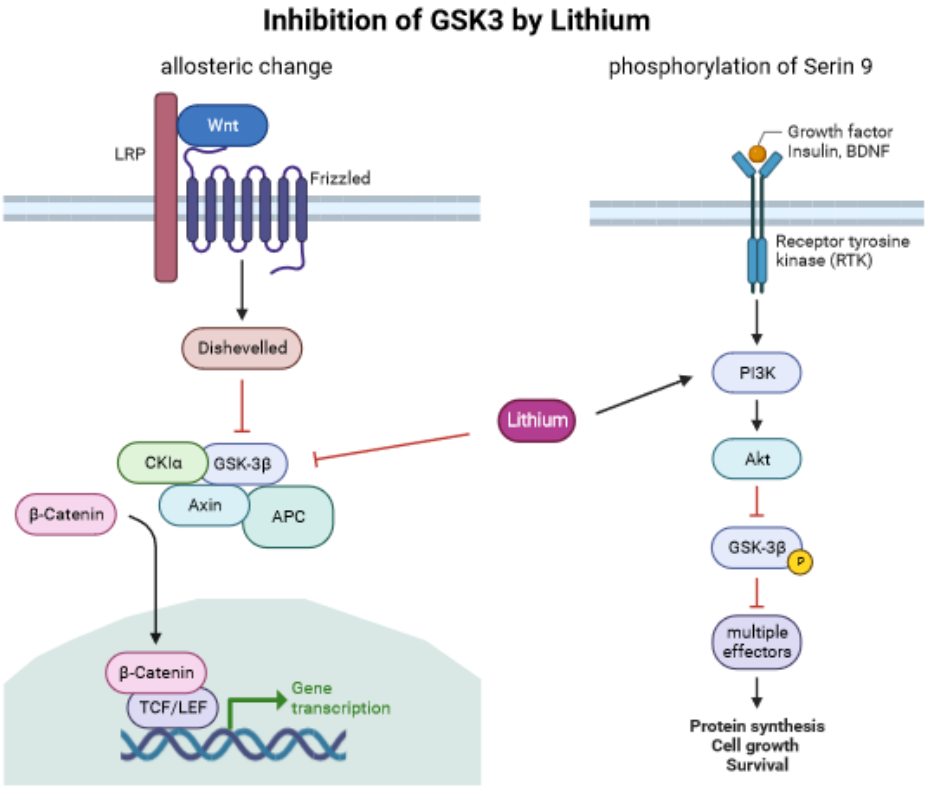

Figure 4: Direct and Indirect Inhibition of GSK3β by Lithium chloride

The figure above shows how lithium can inhibit GSK3β. It, therefore, can mimic the WNT pathway leading to an allosteric change or the PI3K-Akt pathway leading to its phosphorylation.
It is inspired by [35] and created using biorender.

On the other hand, the less characterised non-canonical pathway unites two types, the WNT/PCP and the WNT/Ca^{2+} pathway, which also display a variety of functions. Different WNT ligands bind again to FZD receptors and a co-receptor, determining the exact pathway and the interaction with other proteins like DVL or heterotrimeric G proteins [32]. For the PCP pathway, FZD interacts with tyrosine kinase co-receptors, activating DVL and Rac, further activating Rho-associated kinase, which acts on cytoskeleton arrangement [34].
For the WNT/Ca^{2+} pathway, FZD interacts with heterotrimeric G-proteins, leading to the activation of the phospholipase C and the increase of cytoplasmic Ca^{2+} levels. It then results in the activation of Ca^{2+}-dependent proteins and transcription factors [33]. In adult brains, WNT/Ca^{2+} takes part in LTP [33].

An imbalance between the canonical WNT pathway and the WNT/PCP leads to synaptic loss, especially in the hippocampus, and impaired LTP leads to memory impairment and cognitive decline, as observed in mice [29]. As described above, the correct function and assembly of the presynaptic region require canonical WNT signalling, while the postsynaptic region relates to the non-canonical WNT signalling [33]. Studies showed before that Aβ interferes with postsynaptic proteins like postsynaptic density protein 95 (PSD95) and receptors like AMPA and NMDA. Thereby reducing the capability of LTP and disturbing the balance of the synapse [39]. Aβ also decreases the synaptic function due to inhibiting the WNT signalling by inducing GSK3β activation and Dickkopf-related protein 1 (Dkk1) upregulation [26], [27]. Dkk1 is a WNT antagonist binding the lipoprotein receptor-related protein 6 (LRP6) co-receptor and inhibiting the canonical path, leading to a more significant imbalance in the synapse region and resulting in synapse loss [29], [40].
Researchers found that the interconnection between WNT and Aβ is circular, especially the inactive canonical WNT favours the amyloidogenic pathway. β-catenin in the nucleus inhibits the transcription of BACE and the amyloidogenic pathway. The product of the non-amyloidogenic pathway also reduces GSK3β activity, leading to more β-catenin reaching the nucleus. On the opposite side, Aβ upregulates GSK3β therefore increasing the degradation of β-catenin leading to more BACE and Aβ production. Dkk1 upregulation also leads to an increase in the amyloidogenic product due to the inhibition of the canonical pathway [28].
The canonical WNT signalling pathway also plays a role in the formation of tau tangles. GSK3β is a kinase that can lead to tau hyperphosphorylation, while hyperphosphorylated tau can increase GSK3β activity by oxidative stress and apoptosis [41]. Figure 6 displays an overview of these interactions.
Studies have found that activating the canonical WNT pathway can reverse some effects of Dkk1 upregulation and improve the overall synaptic condition. Researchers saw that increased WNT signalling has protective functions against Aβ neurotoxic effects. The increase in WNT signalling to prevent AD-negative changes comes with a considerable risk of developing cancer since many WNT genes play an enormous role in cancer [29].

1.3 Molecular aspects and role of Mitochondrial unfolded protein response

As mentioned before, AD is an ageing-related disease, and Aβ, as well as tau, play a role within the complete nervous system, which is sensitive to changes, especially proteotoxic stress from misfolded proteins during ageing [42]. It is not yet fully understood why higher age disturbs the balance between misfolded and native proteins. This disturbance is one main reason for many neurodegenerative diseases. It is often accompanied by peripheral illness, which disturbs the metabolism and other cellular functions [42]. Cell compartments develop different stress responses to prevent cell death, increase fitness, and increase the chance of survival [42]. Impaired mitochondria activate the mitochondrial stress response

to counteract these disturbances [7], [43]. The lifespan of Aβ positive C. elegans increased with the activation of mtUPR, leading to a connection with AD [44]. Therefore, researchers propose the mitochondrial cascade hypothesis, which says that mitochondrial failure could be the primary cause of sporadic AD [45].

1.3.1 Defining mitochondrial unfolded protein response

Unfolded protein response is a signalling transduction pathway activating the expression of genes needed for protein handling and improving compartment function [46]. To prevent toxic or damaging actions by misfolded proteins, cells need chaperones and proteases, which influence the capacity for correct folding and degradation [46], [47]. This capacity is essential for maintaining an equilibrium between unfolded or misfolded proteins. The native folding of proteins in organelles depends on the environment [46], [47]. Researchers first studied the unfolded protein response in the endoplasmic reticulum (ER) but also discovered its presence in mitochondria [46], [47].

Mitochondria are responsible for various functions like producing ATP during the tricarboxylic acid cycle and oxidative phosphorylation, taking part in different signalling pathways, and regulating cellular metabolism. Malfunction of mitochondria leads to a decreased life span and is the cause of many diseases [48]. During evolution, multiple mitochondrial stress response pathways developed to increase the fitness of an individuum and to cope with changes in the surroundings of the mitochondria [49]. Mitochondrial protein quality control is the overall quality control system. It monitors different aspects of proteins in mitochondria, like synthesis, transport, and degradation, to ensure correct functioning [48].
Cell compartments need to communicate to regulate function. Since the mitochondrial genome encodes only 13 proteins needed for mitochondrial stability and function, it requires the nucleus to transcribe many proteins, which are then translated into the cytoplasm [50]. The transport of these proteins into mitochondria occurs in an unfolded state, and proteins then need to be folded into their native structure [50]. This process relies on highly conserved machinery, including various chaperones such as heat shock protein 60 (Hsp60) or mitochondrial heat shock protein 70 (mtHsp70) [50]. In case of mistakes, the mitochondria need proteases, which can be either located in the intermembrane space or the matrix, like caseinolytic mitochondrial matrix peptidase (ClpP) and LON protease (Lonp) [50].
Mitochondrial unfolded protein response (mtUPR) is one part of the mitochondrial protein quality control system, and it is a retrograde signalling pathway between the mitochondria and the nucleus [47]. The main consequence of mtUPR activation is the increase of mitochondrial chaperones due to misfolded proteins. It also increases the expression of proteases and protein importers [50]. Mitochondrial stressors, like an increase in the concentration of misfolded proteins, oxidative stress, or DNA depletion, lead to the activation of mtUPR. Other triggers can be stress responses in the cytosol, overexpression of chaperones, or the knockout of specific proteases [43]. The different changes due to the activation of mtUPR can lead to an improvement during disease because of the increased organismal fitness [43], [47], [49], [50].

1.3.2 The activation of the Mitochondrial unfolded protein response and its consequences

Figure 5 displays the interconnection of mammalian mtUPR with the integrated stress response (ISR) and compares it with the mtUPR in C. elegans. Despite being found in mammalian cells, it is much less well-described than mtUPR in C. elegans [51].

ISR is a eukaryotic stress response that reduces translation while selected genes needed for adaptation start to be translated or upregulated. This process benefits cell survival and initiates apoptosis if survival fails [52]. In mammals, the ISR is a precursor sign of the mtUPR due to the phosphorylation of eukaryotic translation initiation factor 2 alpha (eIF2α), which increases the translation of transcription factors like C/EBP Homologous Protein (CHOP) and Activating transcription factor (ATF) 4 [43]. In C. elegans, ISR often, but not always, appears together with mtUPR[43], [52].
The increase of unfolded or misfolded proteins within mitochondria activates mtUPR. The consequence is a reduced import of new proteins and the start of a signalling cascade to the nucleus to increase the transcription of proteins needed for protein handling and import. A possible treatment for mitochondrial diseases in *Saccharomyces cerevisiae* could be the global reduction of translation [43].
Previous studies found that ATF5, a transcription factor important in mtUPR, interacts with the transcription factors CHOP and ATF4, showing the connection between mtUPR and ISR [51].
ATF5 is the mammalian orthologue and functional analogue of stress-activated transcription factor (ATFS-1) in C. elegans [51]. Both have a weak mitochondrial targeting sequence (MTS) and a nuclear location sequence (NLS) [51].
Figure 5 shows the mtUPR pathway in C. elegans and mammals, and Table 1 lists the differences and similarities in factors between mammals and C. elegans. The process in mammals is similar to C. elegans except for the strong interconnection with ISR [52].

In healthy C. elegans, ATFS-1 is imported into the mitochondria, interacting with DNA polymerase γ and helps replicate the mtDNA. However, Lonp1 degrades it in the mitochondrial matrix. The exact mechanisms and functions of ATFS-1 in the mitochondria are not yet known [53].
The activation of the mtUPR pathway decreases mitochondrial import. Therefore, ATFS-1 translocates to the nucleus via its NLS due to the weak MTS [51]. Lonp1, ClpP or other Proteases degrade unfolded or misfolded proteins in mitochondria, and HAF-1, a matrix peptide exporter in mitochondria, exports them to the cytosol. These degraded fragments accumulate in the Cytosol. This process activates ubiquitin-like protein 5 (UBL-5) and the transcription factor Homeobox protein DVE-1 or Defective proventriculus homolog protein (DVE-1). Ubiquitin-like protease 4 (ULP-4) desumoylates ATFS-1 and increases the import to the nucleus. UBL-5 and DVE-1 also translocate and build a complex with ATFS-1. This complex increases the transcription of proteases, chaperons, heat-shock proteins and mitochondrial importer proteins [43], [47], [49], [50], [51].

The difference in mammals is that m-AAA protease 1 (OMA1), a stress-induced protease, also cleaves proteins within mitochondria, and it is not yet clear which protein exports the protein fragments. OMA1 also cleaves DAP3 Binding Cell Death Enhancer 1 (DELE1), a small protein needed for eIF2α phosphorylation, which leads to an ATF4 increase [54]. ATF5 also interacts with ATF4 and CHOP. Researchers tried to explain the exact connection between ATF5 and ISR-related ATF4 and CHOP [51]. They proposed that ATF4 activates the transcription of CHOP, which then activates the transcription of ATF5 during unfolded protein response in the ER [51]. However, researchers detected ATF5 even six months before an increase of ATF4 in mice during ISR [43]. They showed likewise that many mtUPR target genes contain a CHOP binding sequence in their promotor and that all three transcription factors are part of ISR [43], [51].

Table 1: Shows the different factors in mtUPR
It highlights the difference between mammals and C. elegans *[49].*

	C. elegans	Mammals
Transcription factors	ATFS-1	ATF4 / ATF5 / CHOP
Proteases	ClpP, Lonp1	ClpP, Lonp1, OMA1
Target genes	Hsp 10/60/ mtHsp70	Hsp10/60/mtHsp70

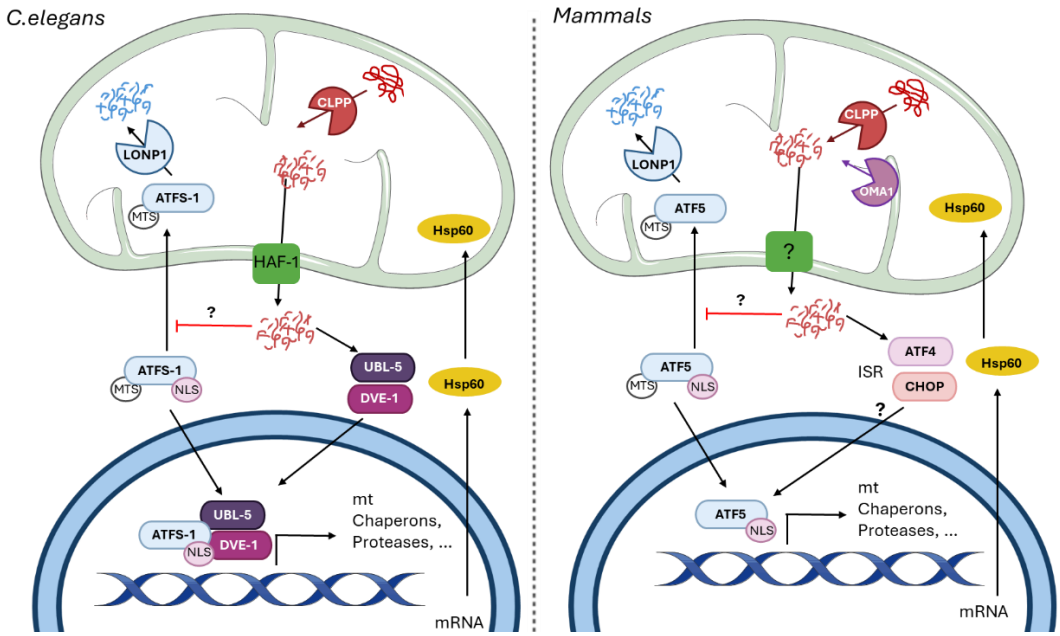

Figure 5: The mtUPR pathway and its key players increase gene transcription in C. elegans and mammals
The above figure shows the mtUPR in mammals and C. elegans. It also displays the differences and open questions. This figure is inspired by the papers [48] and [50] and created with PowerPoint and servier medical art graphs. The left side displays the pathway in C. elegans. It shows the leading players in degradation, like Lonp1 and ClpP. ATFS-1 translocates into healthy mitochondria and to the nucleus during mtUPR. ATFS-1 then interacts with UBL-5 and DVE-1 to increase the transcription. The right side shows the mammalian pathway. The pathway is similar to C. elegans. However, the protease Oma1 in the inner mitochondrial membrane is essential, and ATF5 is responsible for protein transcription, along with the IRS proteins ATF4 and CHOP.

1.3.3 The role of mtUPR in Alzheimer's disease

Previous studies showed that during Alzheimer's progression, many mitochondrial functions like ATP synthesis, Ca^{2+} homeostasis, protein import and oxidative phosphorylation fail [7]. Furthermore, Mitochondrial respiration decreases, morphology changes, and upregulation of mitochondrial stress pathways occurs [44]. In human patients with mild cognitive impairment, genes of the mtUPR pathway, like Hsp60, increased, and in mice, researchers found increased protein levels of ClpP and Lonp1 [44]. The activation of mtUPR reduces developmental and growth delay in Aβ positive C. elegans strains, and researchers observed a correlation between increased mtUPR activation and the increase in lifespan of these worms [44]. These experiments were conducted in the early stages of cognitive impairment and hint at mtUPR as an early sign of AD.
Additionally, previous research suggests that mtUPR plays a role in neuronal and synaptic loss [44]. Previous research saw that the interference with the electron transport chain in mitochondria increases phosphorylated tau and shifts the cleavage of APP to the amyloidogenic pathway. Also, an increase in reactive oxygen species production increases the activation of BACE, leading to more Aβ. Due to this connection between mitochondria, tau, and Aβ, Swerdlow et al. formulated the mitochondrial cascade hypothesis [45].

The mitochondrial cascade hypothesis says that the change in mitochondrial morphology due to its dysfunction leads to further consequences if not adequately compensated by other cell structures [45].
These consequences can be misfolding and aggregation of proteins and neurodegeneration due to metabolic failure. The hypothesis also proposes that mitochondrial failure could be the primary cause of sporadic AD due to decreasing mitochondrial function during ageing and the resulting morphological and biochemical changes [45]. Swerdlow et al. proposed the connection between maternal Alzheimer's disposition and the higher risk in children. The mtDNA is only inherited maternally, while the nuclear DNA comes from both parents. Therefore, the maternal genome strongly influences mitochondria. The mitochondrial cascade hypothesis can explain why late-onset AD does not show a Mendelian inheritance [45].
Figure 6 shows the interconnection of the different players. It displays the interconnection between mtUPR, tau, Aβ and WNT. Not only is the impairment of the mitochondrial electron transport chain proteins influencing Aβ plaques or tau tangles. Nevertheless, hyperphosphorylated tau and Aβ increase oxidative stress and metabolic changes like calcium deregulation, leading to mitochondrial impairment [7].

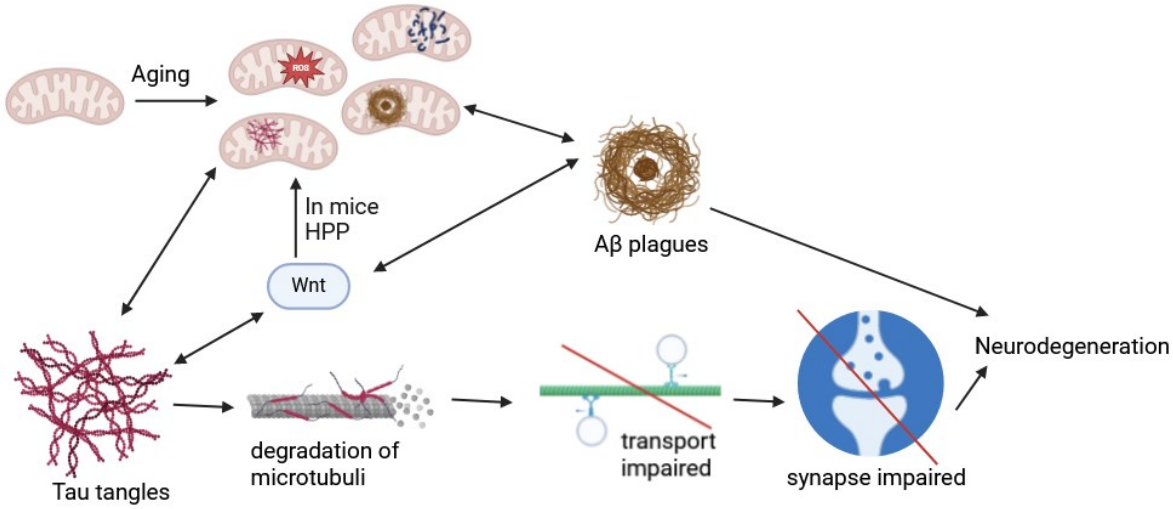

Figure 6: Aß and tau, as well as the connection with WNT and mtUPR
The figure above visualises the interconnection between Alzheimer-related changes and mitochondrial impairment. It is inspired by [45] and created using biorender.

In neurons, there are two types of mitochondria: synaptic and non-synaptic. Controlled neurotransmission, long-term potentiation, and hippocampal memory formation need synaptic mitochondria [7]. The impairment of these functions could contribute to neuronal loss and synapse dysfunction in AD. Synaptic mitochondria display an earlier loss of function than non-synaptic [7]. In AD, more impaired stationary mitochondria are present due to hyperphosphorylated tau, impairing the movement of transported structures, like mitochondria, and decreasing the transport velocity [7], [55].
APP and Aβ increase in AD patients and accumulate in mitochondria after the import via the translocase of the outer membrane (TOM) complex. Soluble fragments and full-length Aβ peptide can then permeabilise the mitochondrial membrane, leading to calcium influx and cytochrome c release, resulting in cell death [7]. On the other hand, APP can bind to translocase of the inner membrane (TIM) and inhibit protein import. Impaired mitochondria lead to more Aβ, resulting in a vicious cycle. Also, in mice, the accumulation occurs earlier in synaptic mitochondria, leading to synaptic dysfunction before AD

histopathological hallmarks. Therefore, the dysfunction of synaptic mitochondria could be an early sign of AD [7].
Tau can also mediate mitochondrial dysfunction despite their interaction being less understood. It can be abnormally located in mitochondria, leading to fragmentation and dysfunction. Tau also reduces mitochondrial membrane potential and oxygen consumption [7]. The knockout of tau prevents synaptic dysfunction and memory impairment in mice, and the mitochondrial impairment due to tau occurs before AD histopathological hallmarks [56].
Mitochondrial changes occur during normal ageing, leading to more sensitive synaptic mitochondria. Ageing modifies Tau and Aβ without AD development and can interact with the mitochondria [7]. Research showed in mice that improving synaptic mitochondria function correlates with better hippocampus memory [57].
Also, dysfunctional mitochondria can interact with tau and Aβ, two essential proteins in AD, leading to morphological changes in the brain. Mitochondrial impairment, therefore, seems to be strongly connected to AD and analysing the effects of mitochondrial stress response on AD progression can improve the condition of mitochondria. Researchers hypothesized that the accumulation of tau and Aβ and the impaired distribution of mitochondria could be an early event before histopathological hallmarks in AD [7].

1.3.4 Recent findings on the relation of WNT signalling and mtUPR

Due to the strong interaction of mtUPR and AD as well as between AD and WNT, researchers analysed the connection between WNT and mtUPR in C. elegans [7], [29]. EGL-20, a canonical WNT ligand, leads to a suppression of cell non-autonomous mtUPR when mutated. In the case of egl-20 knockout, no mtUPR initiation was possible, and hsp-6 was reduced [42], [58], [59]. The gene hsp-6 increases during mtUPR in C. elegans. It is homologous to hsp9A in mammals and encodes the protein mtHSP70. Consequently, researchers often use it as a transcriptional reporter when fused with a green fluorescent protein [60].
Further analysis showed that EGL-20 impairs the stabilisation of β-catenin, which activates mtUPR. Further, they found that cell-autonomous and cell-non-autonomous mtUPR need retromer-dependent WNT signalling to distribute the signal of mtUPR [42], [48]. Researchers showed that in C. elegans, WNT signalling can pass down neuronal mitochondrial stress to the offspring by increasing the mtDNA in germ cells [61].

1.4 Aim of thesis

As indicated above, WNT signalling and mtUPR interact with tau and Aβ and, therefore, with AD. A better understanding of the molecular aspects of the pathways critical for AD can help find future treatment options. Therefore, this thesis investigates mtUPR activation by WNT in SHSY5Y cells and mice brains treated with LiCl and analysed by Western blots.
SHSY5Y cells function as an in vitro neurodegenerative model. They have a neuron-like morphology and can differentiate into mature neurons. They do not demand difficult and expensive care [62], [63], [64], [65]. For the investigation, mice act as an in vivo model. The benefits of mice are their similarity to humans and human diseases and that they are small and, therefore, easier to handle [66].
Researchers have previously treated both SHSY5Y cells and mice with LiCl, showing an activation of WNT signalling. It is an approved drug for bipolar disorder, which is beneficial in case of future use in humans [67].

2 Results

2.1 Analysing the Promotor of mtUPR genes to investigate a possible WNT regulation

The analysis of the promoters of mtUPR genes aimed to identify TCF and LEF elements in human and mouse genes to find a potential for WNT regulation. In the presence of these sites, β-catenin binding is possible and, therefore, WNT regulation [30]. The sequence was obtained by https://www.ensembl.org/index.html [68]. The bioinformatic analysis focused on the 2000 nucleotides upstream of the transcription start site and 500 nucleotides downstream, with a threshold of 80% accordance. The reason for that region is that previous statements explain that most epigenetic markers in promoters are not found outside of the 2000 basepairs (Bp) upstream [69]. Table 2 displays the different numbers of TCF/LEF sequences found per human promotor. The results for mice are in Table 3. The Jasper software can determine between four different sequences for the human species, while there are only two for mice.

Each sequence counts as one binding site, even if two different elements overlap since two or more cannot bind simultaneously. None of the human genes contained a LEF1 binding site in the area investigated. Lonp1 has the least binding sites, while OMA1 has the most. For mice, all genes investigated had similar numbers of binding sites. However, only ATF5 contains zero TCF7 binding sites.

Table 2: Number of possible binding sites of LEF and TCF per promotor in humans
The table shows how often Jasper found a specific sequence for binding the transcription factors (LEF1, TCF7, TCF7L1 and TCF7L2) in a specific human promotor. Sequences of interest had a relative profile score threshold of 80% or more.

	possible LEF1 elements	possible TCF7 elements	possible TCF7L1 elements	possible TCF7L2 elements	Sum
OMA1	0	20	2	6	28
ClpP	0	8	0	14	22
Lonp1	0	7	1	6	14
ATF5	0	10	0	10	20
Hsp60	0	14	7	1	22

Table 3: Number of possible binding sites of LEF and TCF per promotor in mouse
The table shows how often Jasper found a specific sequence for binding the transcription factors (LEF1 and TCF7) in a specific mouse promoter. Sequences of interest had a relative profile score threshold of 80% or more.

	possible LEF1 elements	possible TCF7 elements	Sum
OMA1	4	3	7
ClpP	6	1	7
Lonp1	5	1	6
ATF5	6	0	6
Hsp60	5	2	7

The finding of TCF/LEF binding sites in all mtUPR-related proteins indicates the possibility of WNT regulation. However, the analysis of promoter sequences for TCF and LEF elements can only hint at WNT's regulation. [70]. Therefore, mtUPR proteins were analysed using Western blots in WNT active cells. The first step is the confirmation of WNT activation in cells treated with different LiCL concentrations.

2.2 WNT activation in SHSY5Y cells with different Lithium chloride concentrations

As mentioned in the Aims of the thesis, cells are often used as neurodegenerative models and have neuron-like morphology. Their easy cultivation and frequent use in research are highly beneficial, as well as the low cost of maintaining them [62], [63], [64], [65]. To deactivate GSK3β, Lithium (Li^+) competes with magnesium (Mg^{2+}) and simulates the active WNT pathway [71].

To determine the optimal LiCl concentration for WNT signalling activation, various concentrations (ranging from 1 to 15 mM) and durations (1, 6, and 24 hours) were tested based on literature [72], [73], [74], [75].

To evaluate the activation of the canonical WNT signalling, WNT-related proteins like β-catenin, CamK *IV* and Axin2, as well as GSK3β and the inhibitory state GSK3β phosphorylated on Serin 9 (pGSK3) were measured. Studies found that LiCl treatment increases the phosphorylation of GSK3β on Serin 9 [71]. An increase in these proteins confirmed the correct treatment.

The resulting Western blot data and corresponding graphs (Figure 7, Figure 9, and Figure 10) did not reveal significant changes under any condition. Still, they showed a tendency, which, together with previous research, helped to determine the treatment protocol.

The results of the 1-hour treatment (Figure 7) indicated an increasing tendency in β-catenin (Figure 7C and F), Axin2 (Figure 7C and G) and pGSK3 (Figure 7B and E) for 5 and 10 mM. β-catenin and pGSK3 showed it also with 1 mM of LiCl, but Axin2 did not. The fourth measured protein, CamK *IV* (Figure 7A and D), does not seem to increase with one hour of treatment. The results for 15 mM are less consistent, and cells started to die using 15 mM. A change in their morphology assisted in determining the difference between alive and dead cells. The elongated form of alive cells changed to a round form, and cells decreased in size when dying. Figure 8 displays example pictures.

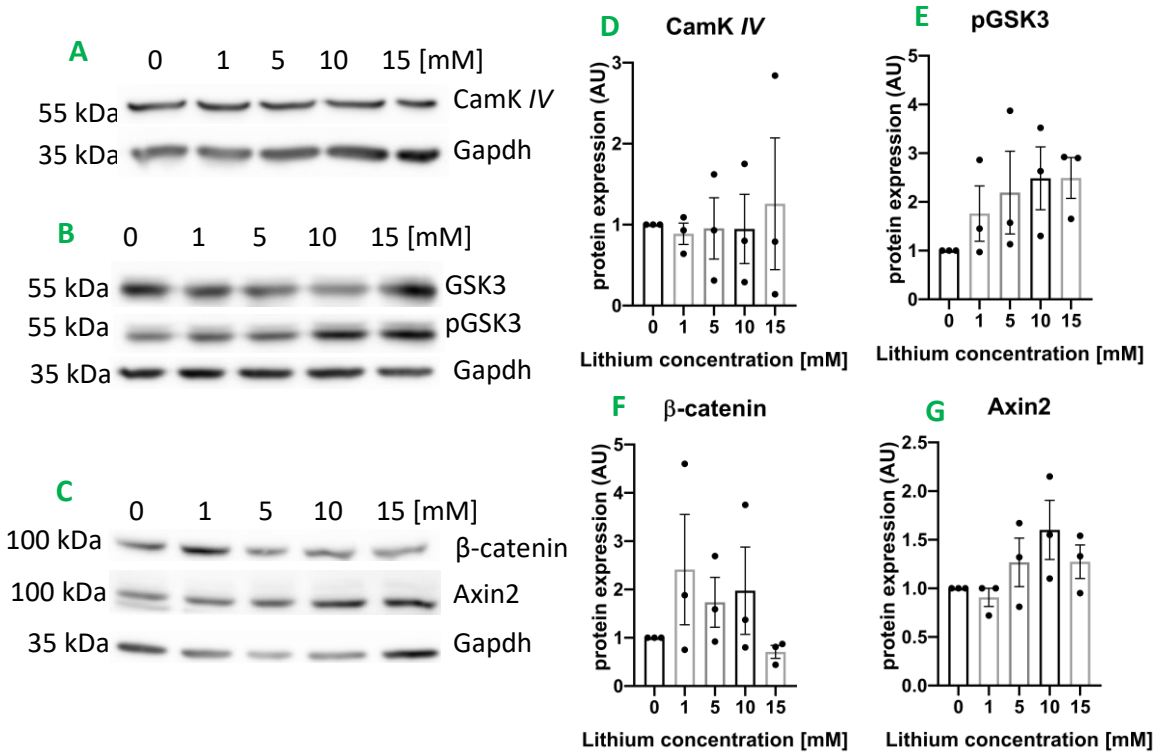

Figure 7: SHSY5Y cells with 1-hour treatment in 5 and 10 mM indicate WNT activation

The plots show the increase and decrease in the WNT protein concentration for 0-15 mM LiCl. For all proteins, GAPDH functions as the Housekeeping. The Number of independent experiments (N) is 3. Statistical analysis was a one-way ANOVA.

A, B, and C show the plots of the WNT proteins and GAPDH as housekeeping.

D is the Graph for CamK IV, E for pGSK3, F for β-catenin and G for Axin2.

pGSK3, β-catenin and Axin2 seem to increase. However, none of the results are significant.

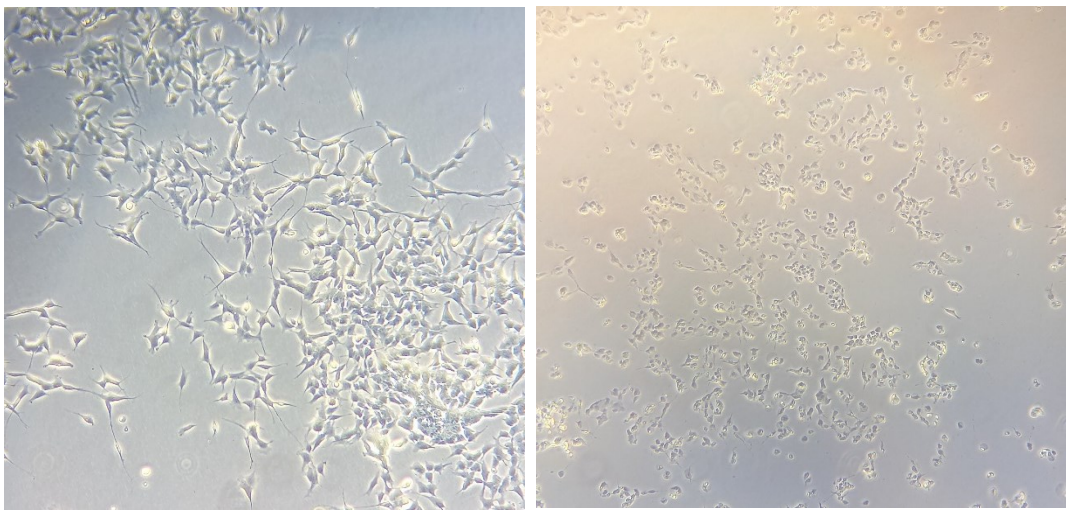

Figure 8: Morphology change of SHSY5Y cells from alive to dead

The figure shows on the left side alive SHSY5Y cells and on the right side dead ones. This morphology change helped distinguish and exclude dead cells from future experiments. Dead cells decreased in size and lost all processes. Both pictures display the cells with a 10X magnification.

The results for the 6-hour treatment (Figure 9) show a higher variability in WNT target genes. Only pGSK3 (Figure 9**B** and **E**) tends to increase in 5 mM and 10 mM. CamK *IV* (Figure 9**A** and **D**) show even a tendency to decrease, and Axin 2(Figure 9**C** and **G**), as well as β-catenin (Figure 9C and F), is not changing. Due to this inconsistency, the 6-hour treatment was not considered for the experiments.

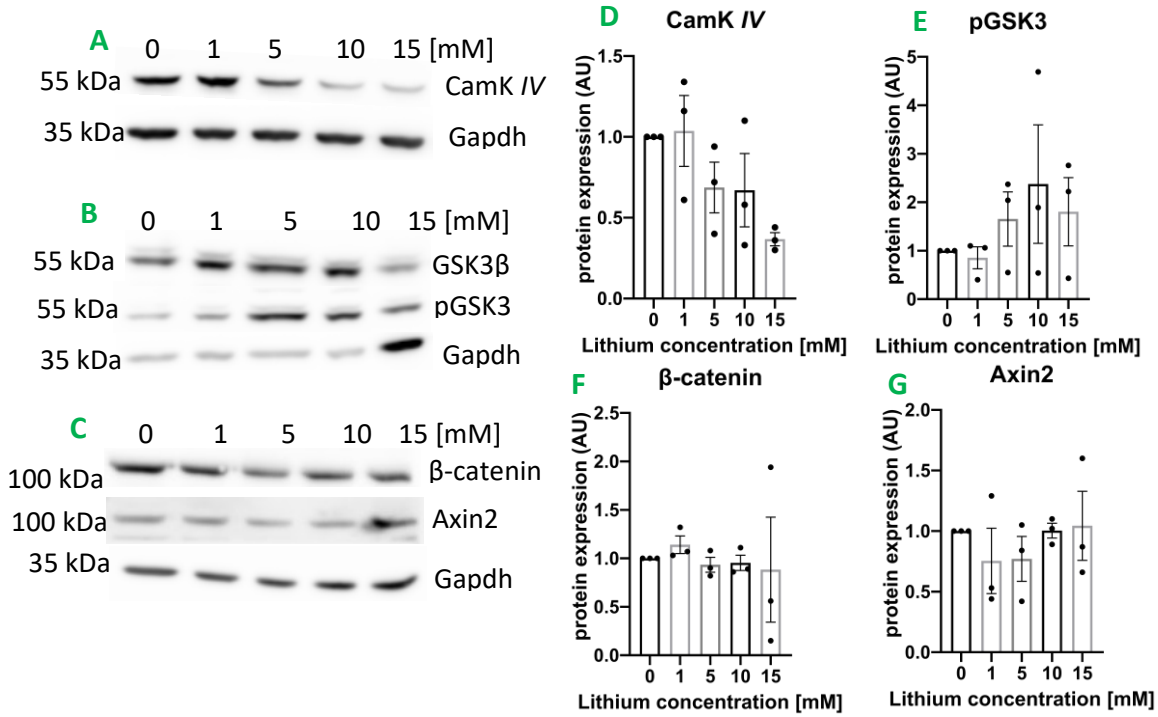

Figure 9: SHSY5Y cells with 6-hour treatment indicating no WNT activation and a high variability
The plots show the increase and decrease in the WNT protein concentration for 0-15 mM LiCl. For all proteins, GAPDH functions as the Housekeeping. N is 3. Statistical analysis was a one-way ANOVA.
A, B, and C show the plots of the WNT proteins and GAPDH as housekeeping.
D is the Graph for CamK IV, E for pGSK3, F for β-catenin and G for Axin2.
Only pGKS3 shows an increase. All other proteins are not changing or decreasing. None of the results were significant.

Compared to the 6-hour treatment, the 24-hour treatment (Figure 10) led to more consistent results with a tendency to increase all proteins except Axin2 in 5 and 10 mM. CamK *IV* (Figure 10**A** and **D**), which showed no increase in the results of 1-hour treatment, was thereby shown to be a late WNT target, which is in accordance with previous results [72]. pGSK3 (Figure 10**B** and **E**) and β-catenin (Figure 10**C** and **F**) tend to increase with all concentrations, but 5 mM and 10 mM showed to be higher than 1 mM and 15 mM. Axin2 (Figure 10**C** and **G**) increased slightly in 1mM and stayed the same in all other conditions.

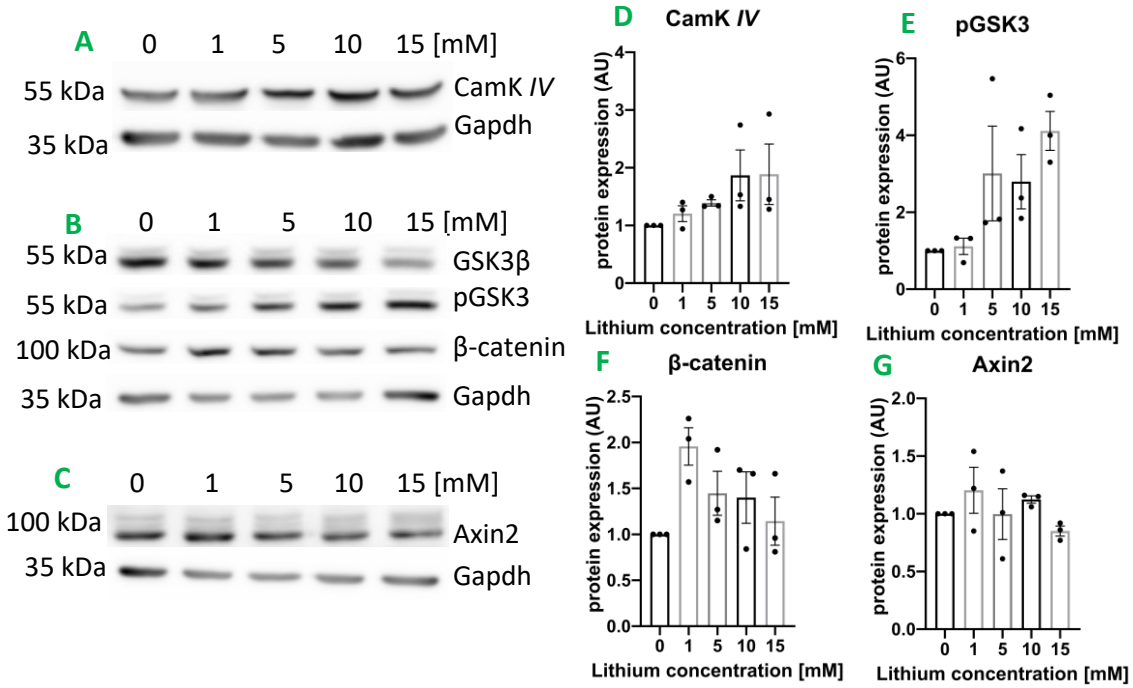

Figure 10: 1, 5 and 10 mM LiCl treatment in SHSY5Y cells with 24-hour treatment indicate WNT activation
The plots show the increase and decrease in the WNT protein concentration for 0-15 mM LiCl. For all proteins, GAPDH functions as the Housekeeping. N is 3. Statistical analysis was a one-way ANOVA.
A, B, and C show the plots of the WNT proteins and GAPDH as housekeeping.
D is the Graph for CamK IV, E for pGSK3, F for β-catenin and G for Axin2.
All proteins suggest an increase; Axin2 showed the slightest increase, and no protein was significant.

Comparing all three treatments, the 6-hour treatment shows the highest variability leading to exclusion. Despite no significant results, 1-hour treatment and 24-hour treatment with 5 and 10 mM for undifferentiated cells indicate WNT activation due to the increase in WNT-related proteins and previous research. Therefore, cells received 0, 5 and 10 mM LiCL for 1 and 24 hours. Further differentiation tests took place to generate more stable results in mature neuronal cells.

2.3 Attempt to differentiate SHSY5Y cells for a stronger neuronal phenotype

The plan involved differentiating the SHSY5Y cells into dopaminergic neurons, as the study focuses on brain cells to uncover new insights for AD. SHSY5Y cells are a human cell line from neuroblastoma and contain two different cell types, the neuronal state and the Schwannian state, which is an epithelial-like type [73]. Previous findings have demonstrated that differentiation with retinoic acid into dopaminergic neurons increases phosphorylated tau and GSK3β levels. This method helps to investigate the hyperphosphorylation and neuroprotective capacity of various substances [62]. Various protocols involve using retinoic acid to initiate differentiation [74]. Researchers have also used only retinoic acid and described a change in morphology and increased neurogenic markers [74].
Consequently, this attempt only involved retinoic acid to differentiate cells. To analyse dopaminergic markers, the examination of the following proteins using western blots occurred: The dopaminergic markers tyrosine hydroxylase (Figure 11**B** and **C**), D2 type dopamine receptor (Figure 11**A** and **C**), and dopamine transporter (Figure 11**B** and **C**) [63] as well as neuronal marker Tau (Figure 11**A** and **D**), MAP2 (Figure 11**B** and **D**) and synaptophysin (Figure 11**B** and **D**). The observations revealed a decrease in most proteins, with only synaptophysin and D2 dopamine receptors showing an increase.

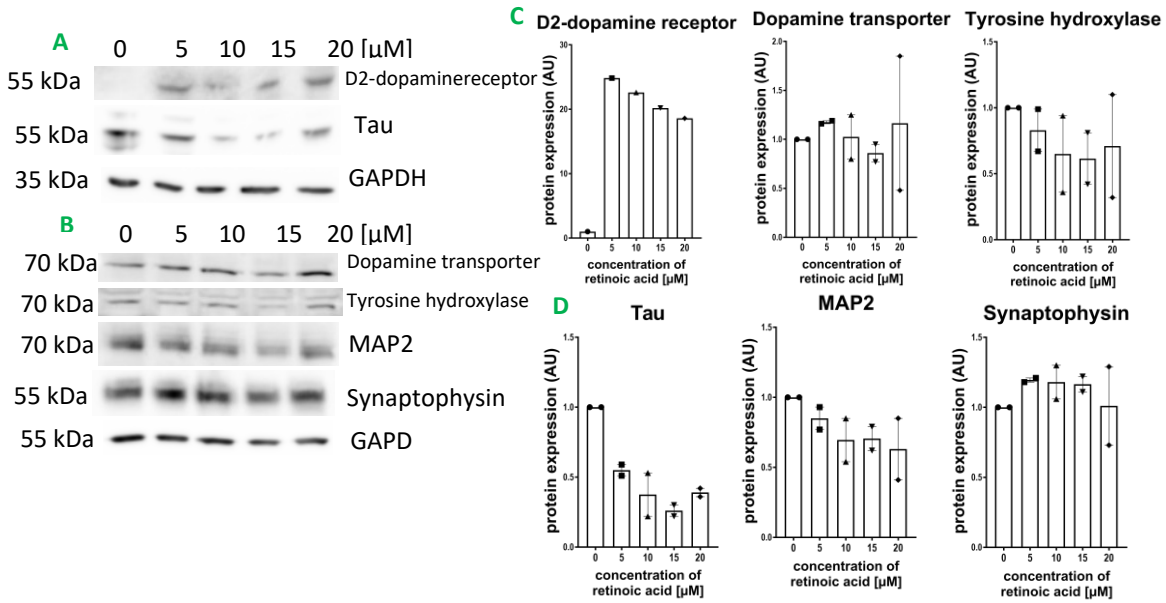

Figure 11: No differentiation, but a phenotypical change occurred in retinoic acid-treated SHSY5Y cells
A and B show the plots of the neurogenic and dopaminergic markers with their housekeeping GAPDH.
C displays the graph for dopaminergic markers, and D the graphs for neurogenic markers.
N is 2, and no statistical evaluation was possible.

The increase of at least two proteins shows a change after the treatment with retinoic acid. Nevertheless, the cells are not jet fully differentiated. The morphology of the cells indicates the same conclusion. Figure 12 shows example pictures of the cells treated with the different concentrations of retinoic acid, which vary between 0 to 20 µM. The increase in retinoic acid changes the morphology of the cells closer to differentiated cells with a more elongated body and projections. However, many cells did not jet develop long projections, and the cells still display a clustering phenotype not seen in differentiated cells. A picture of Xun et al. [75] was used to compare the morphology of these experiments with fully differentiated cells.

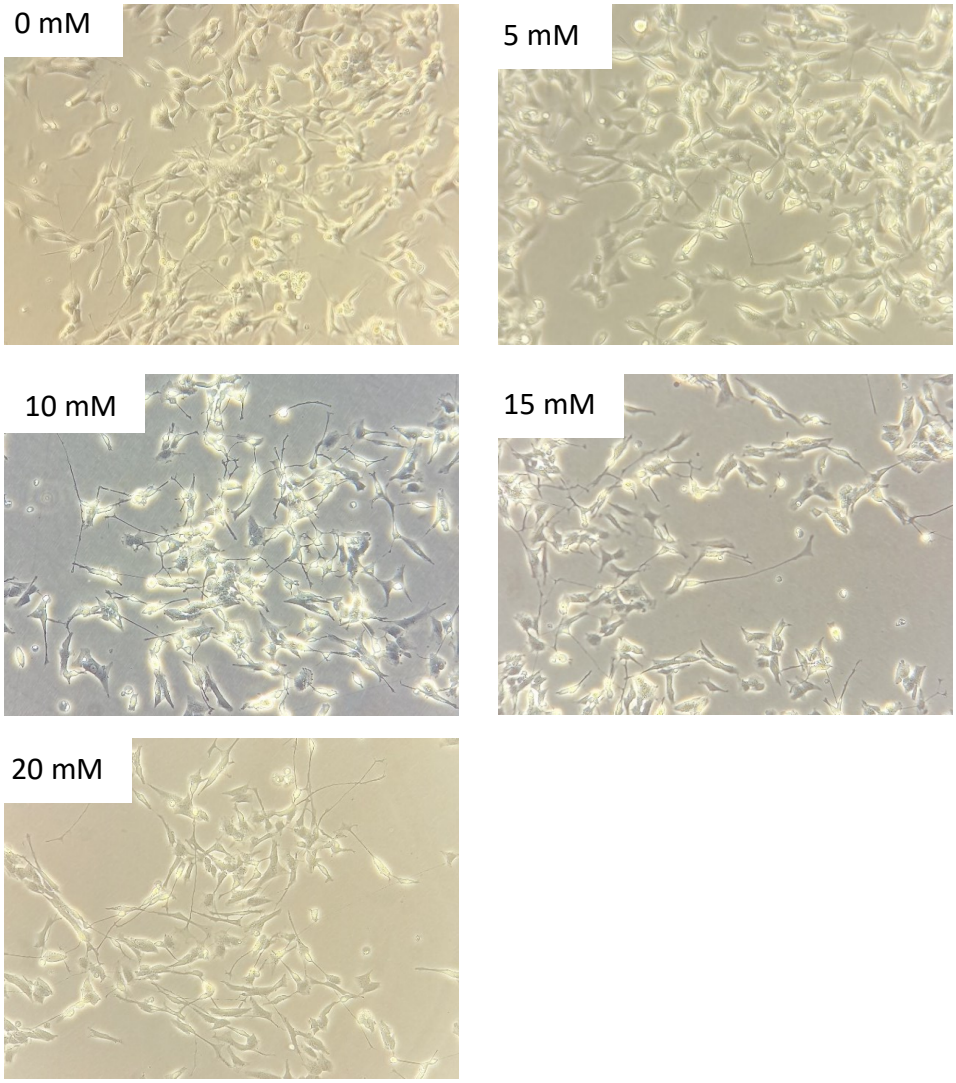

Figure 12: Morphology change of cells treated with different retinoic acid concentrations
The figure above shows the five treatments with retinoic acid. The cells received 0 to 20 µM of retinoic acid for 7 days. All pictures display the cells with a 20X magnification.

The morphological analysis indicates a differentiation by showing a cluster formation and projection development change. However, compared with fully differentiated, it seems to have only started. Western blot results also prove the start of differentiation by an increase of synaptophysin and D2 dopamine receptors. Due to the failure to create fully differentiated cells, the experiments continued with undifferentiated cells.

Since the undifferentiated SHSY5Y cells contain a neuronal-like phenotype, they also contain dopaminergic factors [76]. However, studies found that the passage number could change the composition of the two phenotypes, thereby changing the amount of the different proteins in a sample. A higher passage number can undergo a higher phenotypic drift, which could lead to more variance in the results [73]. On the other hand, a higher passage number of undifferentiated cells expresses more dopaminergic factors [77]. SHSY5Y cells were used in their undifferentiated state until passage 10 to investigate the mtUPR protein levels in LiCl-treated cells.

2.4 Investigation of mtUPR protein levels in WNT active cells

Western blot analysis investigated the mtUPR proteins in cells treated with 0, 5 and 10 mM of LiCl for 1 and 24 hours. To control the WNT activation, analysis of pGSK3 and β-catenin

occurred. To evaluate the activation state of mtUPR, the protein levels of the main transcription factor ATF5 and mtUPR-related proteins were measured. The investigated proteins are proteases like Lonp1, ClpP, and OMA1, as well as the chaperon Hsp60. Western Blot analysis of mitochondrial proteins, Tom20 and voltage-dependent anion channel (VDAC) proved that the observed change is due to the WNT activation and not an overall increase in mitochondrial proteins. Therefore, an increase in mtUPR proteins with an increase in WNT proteins and without an increase in mitochondrial proteins would indicate the WNT and mtUPR connection.

The 1-hour treatment (Figure 13) showed only one significant result in Lonp1 (Figure 13**C** and **F**) between 0 mM and 5 mM with a p-value of 0,0246. For the mitochondrial protein Tom20 (Figure 13**A** and **D**), the tendency is also going up in all conditions, while the mitochondrial protein VDAC (Figure 13**A** and **D**) does not seem to change. Both proteins are not significant. As observed in determining the LiCl concentration, cells again showed highly variable results. There is a tendency for increasing seen in the two WNT-related proteins pGSK3 (Figure 13**B** and **E**) and β-catenin (Figure 13**B** and **E**) in both treatment concentrations. OMA1 (Figure 13**C** and **F**), ClpP (Figure 13**C** and **F**) and Hsp60 (Figure 13**C** and **F**) also show this tendency for 5 mM and 10 mM treatment, while Lonp1 and ATF5 (Figure 13**C** and **F**) show a decrease in 10 mM. However, all of the proteins show a high variance and no significance.

The results for the 24-hour treatment in Figure 14 seem more stable. Two proteins increased significantly, pGSK3 (Figure 14**B** and **E**) in 5 mM with a p-value of 0,0400 and Lonp1 (Figure 14**C** and **F**) in 10 mM with 0,0338. The mitochondrial protein Tom20 (Figure 14**A** and **D**) seems to be increasing, while VDAC (Figure 14**A** and **D**) did not. The WNT protein pGSK3 (Figure 14**B** and **E**) was also almost significant in 10 mM, having a p-value of 0,0599. On the other hand, β-catenin (Figure 14**B** and **E**) shows a tendency to decrease in 5 mM and increase in 10 mM, but this was not significant. The mtUPR protein Lonp1 (Figure 14**C** and **F**) also did not increase much in 5 mM. Comparing 0 mM with 10 mM resulted in other almost significant proteins. Hsp60 (Figure 14**C** and **F**) has a p-value of 0,0505, OMA1 (Figure 14**C** and **F**) has 0,0749, and ATF5 (Figure 14**C** and **F**) has 0,0724. ClpP (Figure 14**C** and **F**) seems to increase in both conditions but shows no significance. The increase is higher when comparing 0 mM with 10 mM within all mtUPR proteins.

The data collected indicate that the activated WNT signalling increases the protein levels of the mtUPR proteins and, therefore, creates a connection between the two pathways.

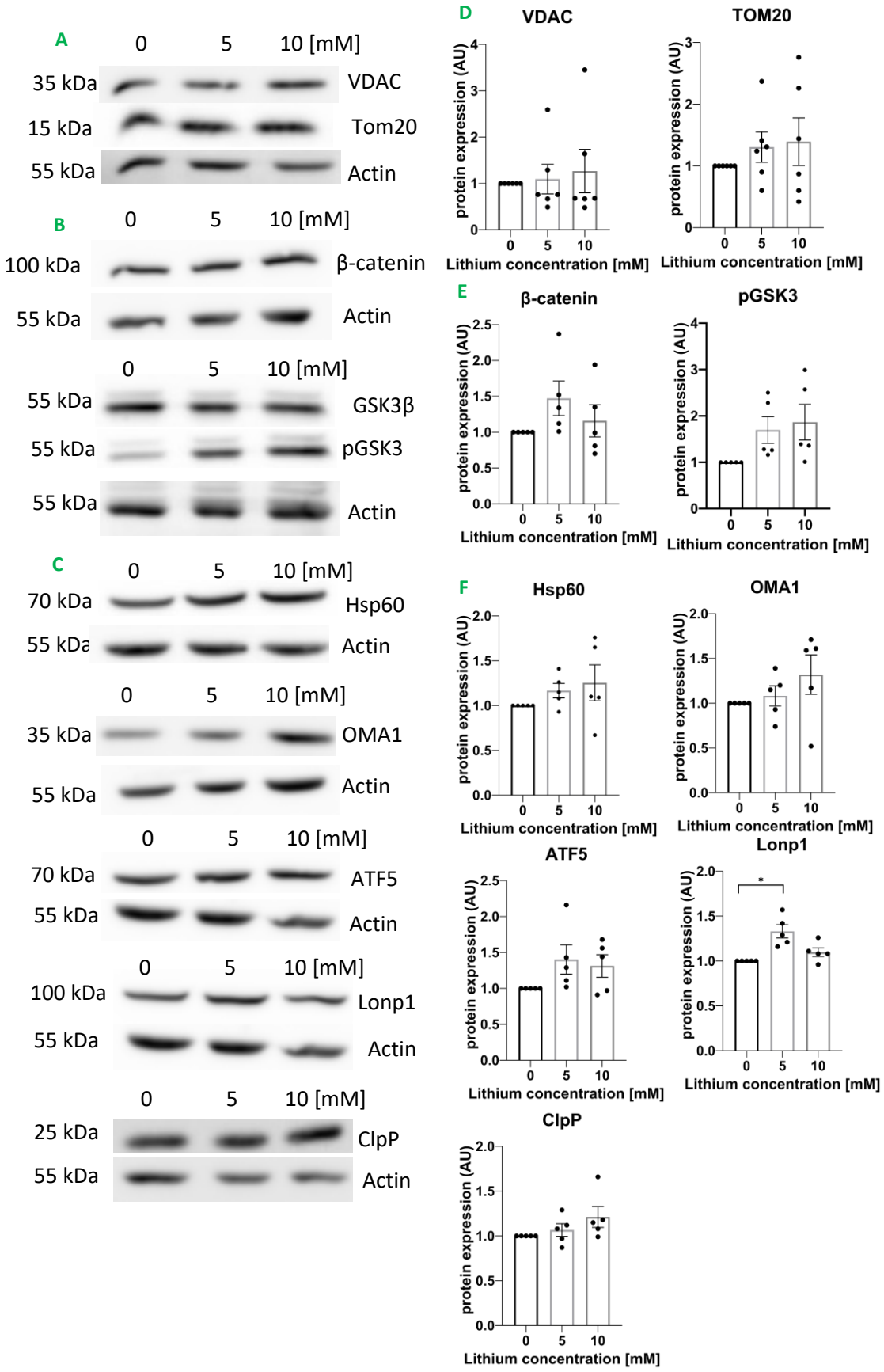

Figure 13: The experiments showed a non-significant increase in WNT and mtUPR protein levels in 1-hour LiCl treatment

*Cells received 0 mM, 5 mM and 10 mM LiCl for 1 hour. * Means having a p-value below 0,05 in a one-way ANOVA. A shows the plots of the mitochondrial proteins, B for WNT proteins and C for mtUPR proteins.*
D displays the graphs for mitochondrial proteins, E for WNT proteins and F for mtUPR proteins.
N is 5.

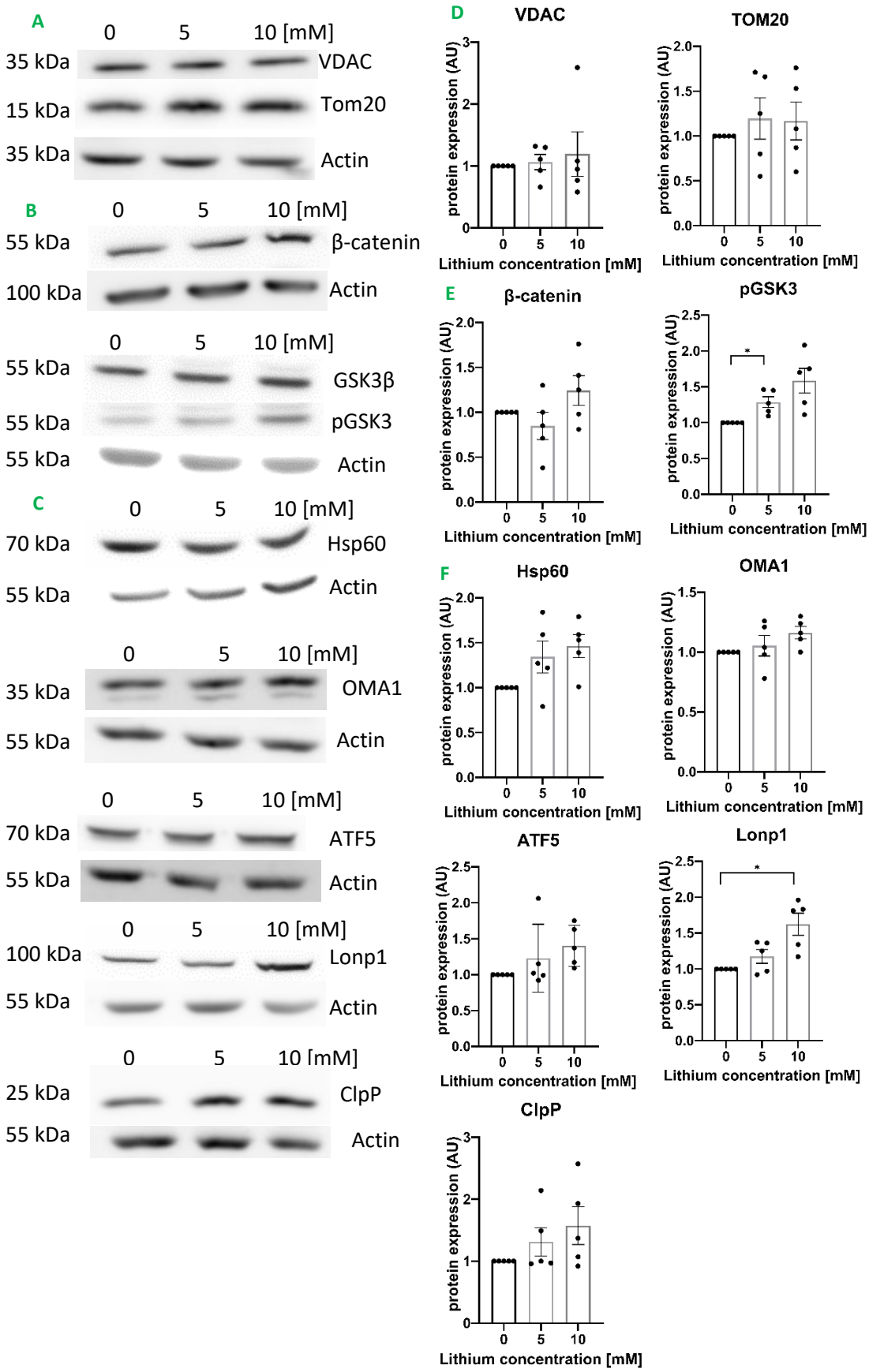

Figure 14: Activation of the WNT pathway indicated increased mtUPR protein levels with 24-hour LiCl treatment
*Cells received 0 mM, 5 mM and 10 mM LiCl for 24 hours. The results indicate an increase of WNT and mtUPR proteins, but only pGSK3 and Lonp1 increased significantly. * Means having a p-value below 0,05 in a one-way ANOVA. A shows the plots of the mitochondrial proteins, B for WNT proteins and C for mtUPR proteins. D displays the graphs for mitochondrial proteins, E for WNT proteins and F for mtUPR proteins.*
N is 5.

Regular morphology checks took place to examine changes by LiCl treatment. Figure 15 shows example pictures of the morphology of cells treated with 0 mM, 5 mM, and 10 mM.

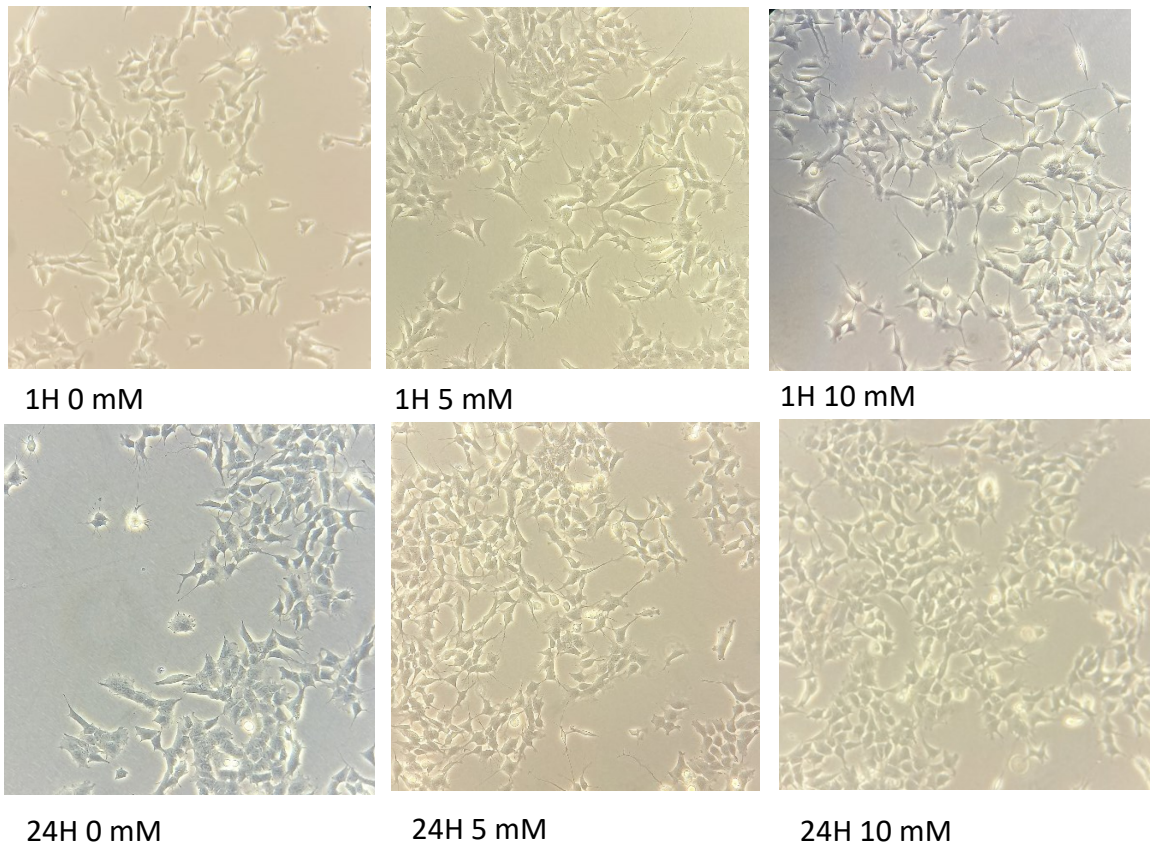

Figure 15: Morphology of cells treated with different LiCL concentrations for 1 and 24 hours
The upper lane shows cells treated for one hour, while the lower lane shows pictures of 24-hour treated cells. All pictures display cells with 10X magnification.

The results of the Western blot analysis indicated that the 24-hour treatment with 5 mM and 10 mM activates WNT signalling. It shows that mtUPR proteins Hsp60, ATF5 and OMA1 are almost significant in 10 mM, and Lonp1 shows a significant increase. Therefore, it suggests that WNT activation can lead to mtUPR activation. The analysis of the translocation of ATF5 and β-catenin required immunohistochemistry experiments. The experiment aimed to investigate if WNT activation leads to the translocation of ATF5 and activation of mtUPR or just an increase in mtUPR proteins without translocation.

2.5 Testing Immunofluorescence analysis in cells to follow the translocation of ATF5 and β-catenin

Immunofluorescence analyses aimed to follow the translocation of ATF5 and β-catenin. β-catenin functions as a WNT activation control. In case of active WNT, the degradation complex does not mark β-catenin for degradation, and it can translocate to the nucleus to start the transcription of WNT target genes [34], [37], [38]. ATF5 also translocate during active mtUPR due to the failure of the import into mitochondria [51]. Therefore, Hoesch and TOM20 antibodies stained the nucleus and the mitochondria, respectively, to figure out the location of ATF5 and β-catenin. Our experiments showed that the antibody used for β-catenin cannot enter the nucleus. Therefore, the WNT activation control failed, and no further immunohistochemistry occurred. Example pictures in Figure 21 and Figure 22 and the method description are in Appendix 8.1 and 8.2. The Appendix Section 8.4 also noted a

Python merging and analysis script. To further analyse mtUPR activation by WNT, mice function as an in vivo model.

2.6 mtUPR protein levels in mice cortex and hippocampus after LiCl treatment

Despite the tendency and variation seen in human cells, the analysis of mtUPR proteins occurred in mouse brain samples. Previous research showed that LiCl could activate the WNT signalling in mice brains [72]. Two sets of eight mice received 2,3 mmol LiCl per kilogram or the same amount of saline solution by intraperitoneal injections. Each group contained four animals. The duration for both sets was two weeks, but the first set received treatment every second day and the second set everyday. Analysed proteins are the two mitochondrial proteins Tom20 and VDAC, as well as the WNT-related proteins pGSK3, β-catenin, CamK *IV*, Axin2 and PSD95 and Lonp1, Hsp60, ATF5 and ClpP as mtUPR-related proteins.

Every second-day treatment showed no significant increase in any of these proteins in the Cortex (Figure 16). In the hippocampus samples (Figure 17), Axin2 (Figure 17**B** and **E**) significantly increased with a p-value of 0,0262, but none of the other proteins showed any significant results. That suggests that every second-day treatment was insufficient to activate the WNT signalling pathway.

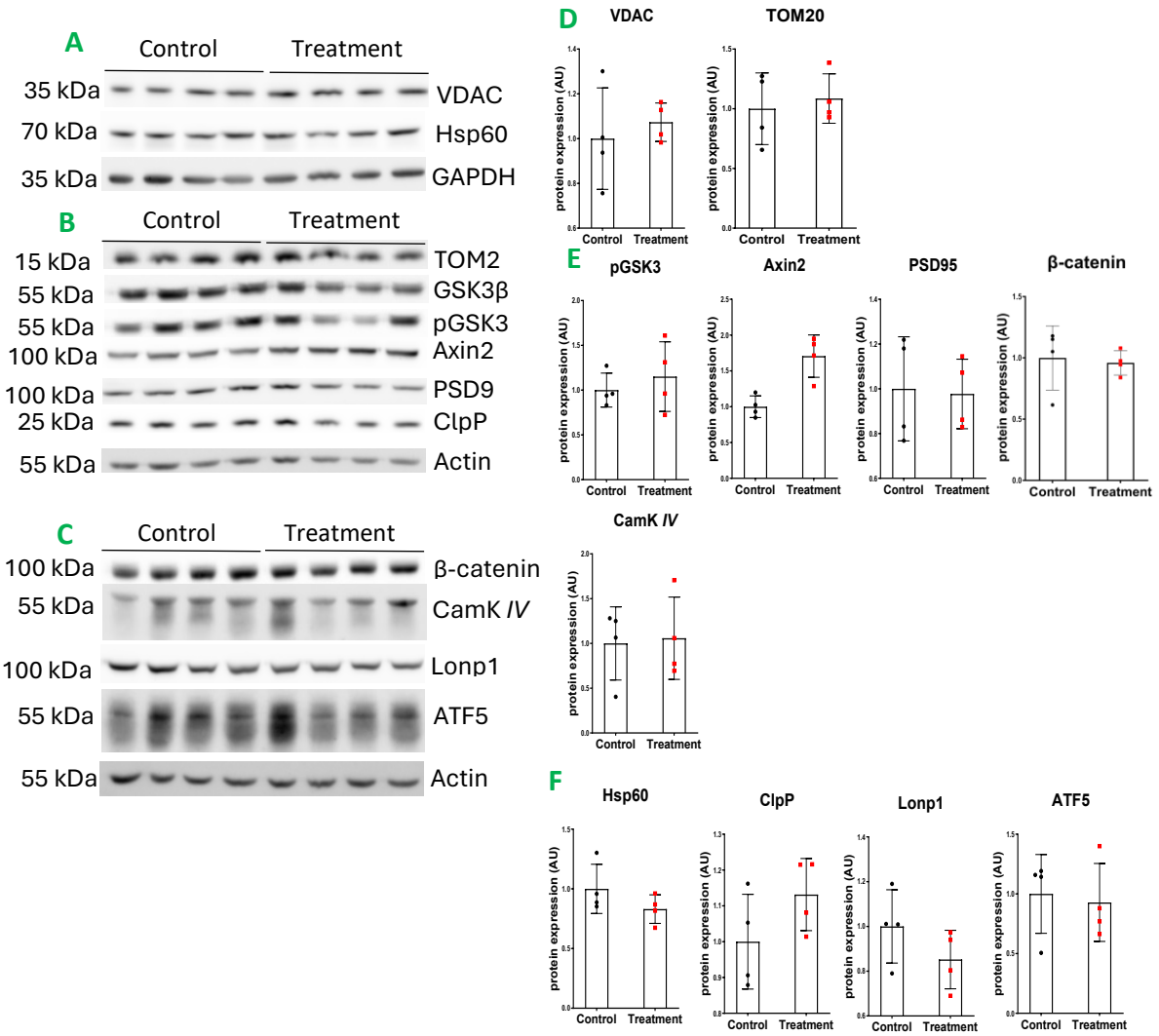

Figure 16: Every second-day treated Cortex samples show no WNT activation

The figure above shows the plots of the WNT, mitochondrial, and mtUPR protein measured in the Cortex samples on the left side and the graphs on the right side.

A, B and C are the plots of mitochondrial, WNT and mtUPR proteins and their housekeeping.

D shows the analysis of the mitochondrial proteins, while E displays the WNT proteins, and F the mtUPR proteins.

** means having a p-value below 0,05. In all mice experiments, the statistical analysis was a t-test. N is 4.*

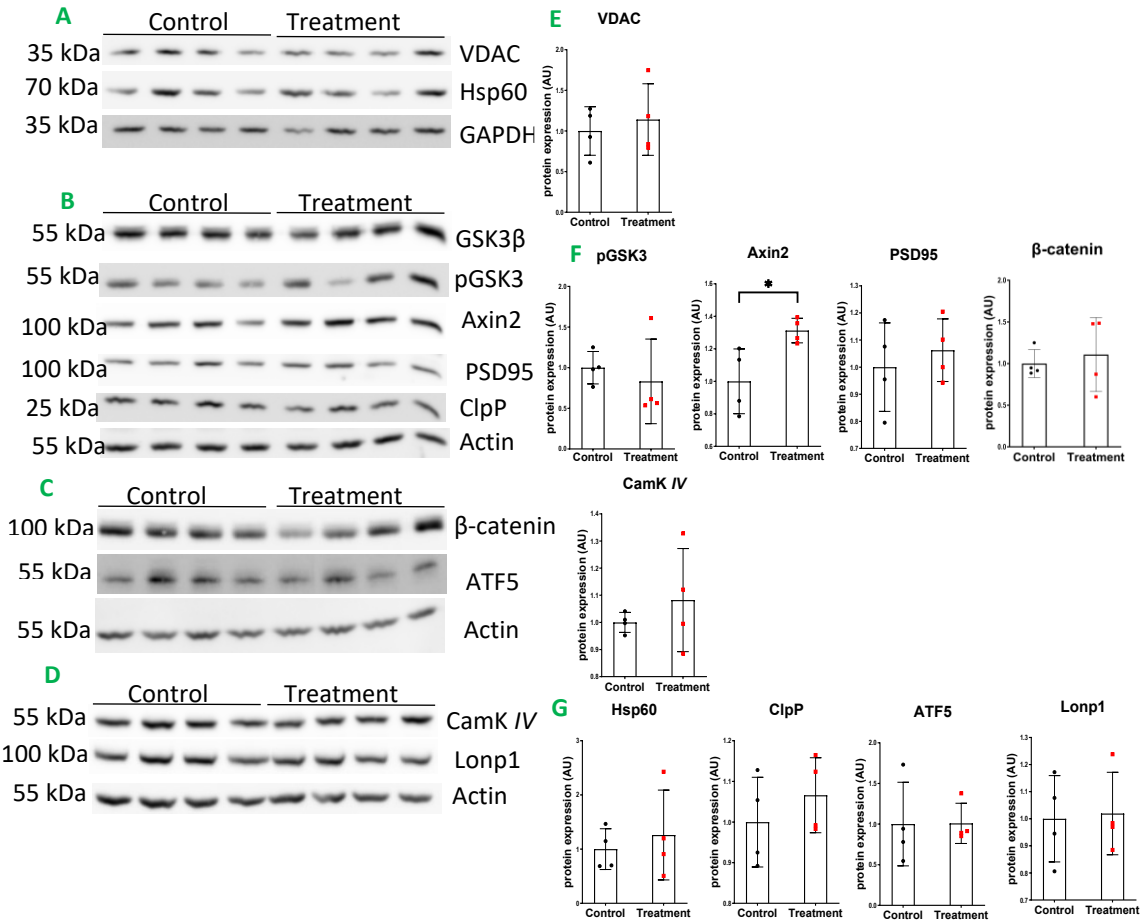

Figure 17: Every second-day treated Hippocampus samples do not prove WNT activation

The figure above shows the plots of the WNT, mtUPR, and mitochondrial protein measured in the hippocampus samples on the left side and the graphs on the right side.

A, B, C and D are the plots of mitochondrial, WNT and mtUPR proteins and their housekeeping.

E shows the analysis of the mitochondrial proteins, while F displays the WNT proteins, and G the mtUPR proteins.

** means having a p-value below 0,05. In all mice experiments, the statistical analysis was a t-test. N is 4.*

Figure 18 displays the results for the cortex of everyday treatment. WNT-related proteins like PSD95 (Figure 18**B** and **E**), CamK *IV* (Figure 18**C** and **E**) and β-catenin (Figure 18**C** and **E**) seem to be increasing. At the same time, pGSK3 and Axin2 (Figure 18**B** and **E**) are stable. VDAC (Figure 18**A** and **D**) stayed the same, and Tom20 (Figure 18**B** and **D**) decreased significantly with a p-value of 0,0256. In the group of mtUPR-related proteins, Hsp60 (Figure 18**A** and **F**) significantly decreased with a p-value of 0,0233, and ATF5 (Figure 18**C** and **F**) increased significantly with a p-value of 0,0403. LONP1 (Figure 18**C** and **F**) seemed to increase but were insignificant, while ClpP (Figure 18B and F) seemed stable. The proteins pGSK3, β-catenin, and WNT target genes (Figure 18**E**) showed no significant increase, indicating no activation of the WNT signalling pathway.

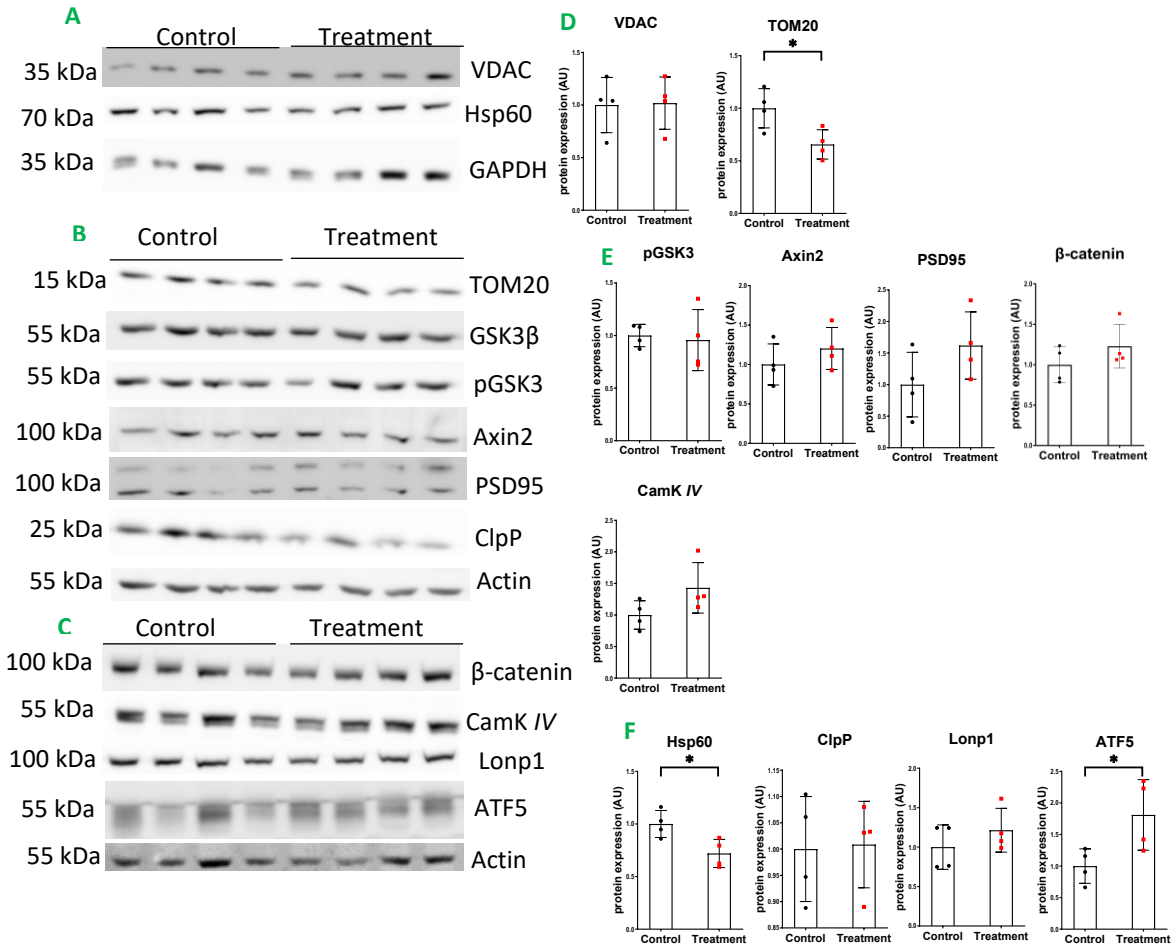

Figure 18: Cortex samples of everyday treatment do not prove WNT activation

The figure above shows the plots of the WNT, mtUPR, and mitochondrial protein measured in the Cortex samples on the left side and the graphs on the right side.

A, B and C are the plots of mitochondrial, WNT and mtUPR proteins and their housekeeping.

D shows the analysis of the mitochondrial proteins, while E displays the WNT proteins, and F the mtUPR proteins.

** means having a p-value below 0,05. In all mice experiments, the statistical analysis was a t-test. N is 4.*

The analysis of the hippocampus from daily treated mice showed activation of WNT signalling (Figure 19). The mitochondrial protein VDAC (Figure 19**A** and **D**) showed no change. WNT proteins like CamK *IV* (Figure 19**C** and **E**) and β-catenin (Figure 19**C** and **E**) significantly increased with p-values of 0,0478 and 0,0288. Other WNT proteins like Axin 2 (Figure 19**B** and **E**) and pGSK3 (Figure 19**B** and **E**) did not significantly increase. The activation phosphorylation on tyrosine 216 of GSK3β (GSK3pY216) (Figure 19B and E) was additionally measured for these samples. The dephosphorylation on this site decreases GSK3β activity, meaning that GSK3pY216 should decrease during WNT activation [78]. These experiments showed a non-significant increase. Western blot results showed increased mtUPR genes except for Hsp60 (Figure 19**A** and **F**). Significant proteins below 0,05 are ATF5 (Figure 19**C** and **F**) with 0,0318 and LonP1 (Figure 19**C** and **F**) with 0,0266. On the other hand, ClpP (Figure 19**B** and **F**) is even below 0,005 with a p-value of 0,0019.

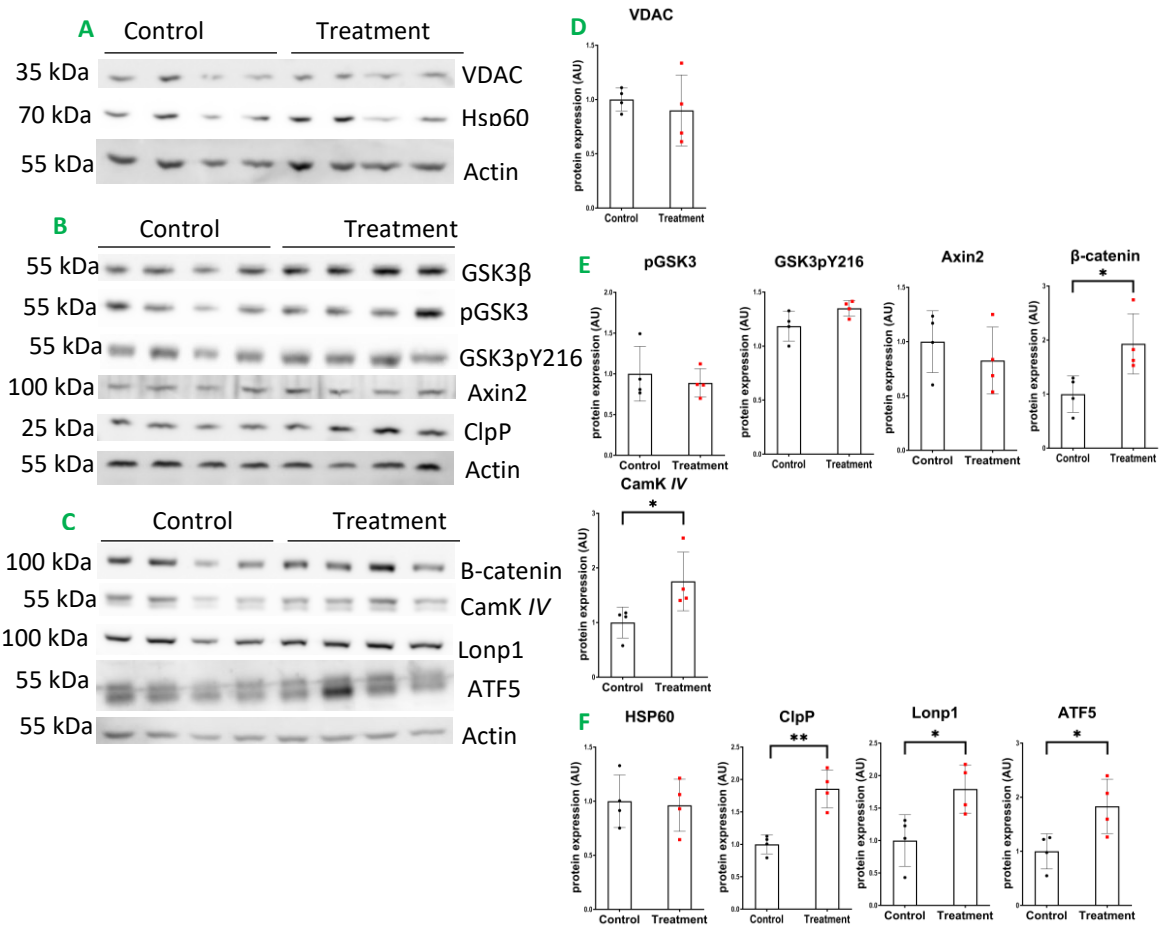

Figure 19: In everyday treated Hippocampus, WNT activation increased mtUPR proteins
The figure above shows the plots of the WNT, mtUPR, and mitochondrial protein measured in the hippocampus samples on the left side and the graphs on the right side. B-catenin and CamK IV increased significantly, indicating the activation of the WNT pathway. Except for Hsp60 mtUPR, proteins significantly increased in the WNT active samples.
A, B and C are the plots of mitochondrial, WNT and mtUPR proteins and their housekeeping.
D shows the analysis of the mitochondrial proteins, while E displays the WNT proteins, and F the mtUPR proteins.
** means having a p-value below 0,05. In all mice experiments, the statistical analysis was a t-test. N is 4.*

The results obtained from mice show that everyday administration can activate the WNT pathway in the hippocampus. It also shows that the hippocampus is more sensitive to the treatment. In the Hippocampus, WNT activation leads to mtUPR activation. Therefore, it reveals that with the correct administration, LiCl concentration and duration, the treatment can activate mtUPR in WNT-activated samples.

3 Discussion

This thesis aimed to analyse the expression of mtUPR-related proteins in WNT signalling active samples to examine the interaction between canonical WNT signalling and mtUPR-associated proteins. WNT signalling has a variety of target genes and plays a significant role in Alzheimer's disease [27]. Within the last years, mtUPR activation increased life expectancy in Aβ positive C. elegans [44]. Researchers found that both pathways interact with the two main proteins in Alzheimer's disease, which are tau and Aβ [7], [28], [41]. Therefore, investigating the connection between WNT and mtUPR can lead to a better understanding of interacting pathways during AD and possible treatment strategies. The choice of lithium treatment was based on its ability to mimic the activation of WNT signalling by inhibiting GSK3β [81]. Secondly, it is already an approved drug against bipolar disorder, which means that other use cases are an expansion and therefore, no

toxicological screen or concentration frame is necessary [67]. Lastly, Chile has central reserves for lithium, which means that the resources are less limited, which is also beneficial due to a low price and faster delivery [82].

To investigate whether WNT signalling can activate the expression of mtUPR-related proteins, a bioinformatics analysis revealed that mtUPR gene promoters contain TCF/LEF binding sites, suggesting potential binding of β-catenin and subsequent regulation by the canonical WNT signalling pathway [34]. Different genes contain varying numbers of binding sequences. However, no correlation emerged between a significant increase in protein and the number of binding sites. Nevertheless, the analysis of promoter sequences for TCF and LEF sequences can only suggest a relationship and a transcriptional increase by WNT signalling. The proof of connection requires further experiments with other methods [70].

Therefore, cells underwent treatment with lithium chloride, which competes with magnesium for the GSK3β binding site and leads to its inactivation [71]. This inactivation of the destruction complex allows β-catenin to translocate to the nucleus and increase the transcription of WNT-related proteins [34], [37], [38]. Sections 2.3 to 2.5 display the cellular results, showing a high variability collectively. Previous research and colleges also observed this variability [63], [77]. SHSY5Y cells come from neuroblastoma and contain two different cell types, the neuronal state and the Schwannian state, which is an epithelial-like type [73]. Neuronal cells are often floating and, therefore, can be discarded with the medium change. To ensure the neuronal state, researchers differentiated the cells into neuronal cells [79].
Previous research performed the differentiation with only retinoic acid [62], [74]. The paper states that there are changes in morphology and dopaminergic-like phenotype [74]. Morphological analysis and Western blots compared undifferentiated and retinoic acid-treated cells to investigate the differentiation process. While the cells in this experiment did undergo morphological changes, they lacked additional processes and appeared more clustered. The cells showed some short processes, indicating the start of differentiation, but also displayed a less elongated body shape. The undifferentiated cells also contain dopaminergic markers, but a successful differentiation would increase them [76]. This treatment only observed this increase in the D2 dopamine receptor and synaptophysin. Other markers, such as dopamine transporter, Tyrosine hydroxylase, tau, and MAP2, are decreasing [63]. These results indicate an incomplete differentiation.
Further research showed that many researchers use reagents like brain-derived neurotrophic factor or phorbol ester [63], [80], which were unavailable in the laboratory. Observing incomplete differentiation led to the decision not to perform repetitions since the significance of the results was irrelevant. Therefore, the study used undifferentiated SH-SY5Y cells, which are also widely used as a neuronal-like cell line, despite the limitations mentioned earlier [69]. The possible different responses of the two cell types could explain the variance seen in the results of mtUPR analysis. Within the 24 hours of treatment, pGSK3 and Lonp1 increased significantly. Oma1, ATF5 and Hsp60 were almost significant, leading to a tendency of increase in mtUPR-related proteins in WNT signalling activated cells.

Despite the observed tendency in cells, researchers treated mice with LiCl and analysed their hippocampi and cortices. The treatment followed published protocols, considering variations among researchers' methods. Based on Xiang et al. and Gould et al., mice received 2,3 mmol/kg LiCl [81], [82] by intraperitoneal injections. The control group received the same amount of a saline solution. The goal was to activate the WNT signalling

pathway and not to treat any condition; therefore, mice received LiCL for a short period of only two weeks, a method previously used by colleagues with lithium carbonate.
Researchers treated mice with acute treatment, which lasted for only one day [82] and chronic treatments lasting for prolonged periods like 30 days [83] or 2 months [81]. Extended treatment periods need everyday administration [81], [83]. The first set of mice received LiCL every second day since Lithium carbonate was sufficient to activate the WNT pathway in this experimental set-up conducted by colleges. However, in this instance, using LiCl every second day did not result in active WNT signalling. Therefore, a second set of eight mice received the treatment daily.
In samples of daily treated mice, WNT proteins did not increase in the cortex but in the hippocampus. As described in section 2.6, CamK *IV* and β-catenin increased significantly in the hippocampus, while Axin2 and pGSK3 remained stable. Similarly, mtUPR proteins like ClpP, LonP1 and ATF5 increase significantly, indicating a connection between WNT signalling and mtUPR-related proteins *in vivo*.
The western blot results show that pGSK3 did not significantly increase.
LiCl leads to a dual inhibition, which is direct and indirect. It inhibits GSK3β by competing with Mg2+ or activating the PI3K – Akt signalling pathway, which is necessary for GSK3β Serine 9 phosphorylation [71]. WNT signalling usually induces the allosteric conformational change, and insulin or BDNF typically induce the phosphorylation of Serine 9 [35]. LiCL-induced GSK3β phosphorylation occurs mainly during chronic treatment. The treatment used was in between the acute one-day treatment and the chronic one [71]. That could explain why these experiments show an increase in WNT-related proteins without an increase in pGSK3.
GSK3pY216, also investigated in the hippocampus of everyday treated mice, is an activation mark which gives more information on the activation state of GSK3β. Previous research observed that LiCl reduces GSK3pY216 [84], but they also noted that LiCl can inhibit GSK3β without altering GSK3pY216 [78] or even by increasing it [85]. Regarding an increase in GSK3pY216, researchers showed that pGSK3 is favoured and inactivated [85]. Here, pGSK3 is not favoured, but WNT-related proteins increased. That indicates an allosteric change leading to the inactivation of GSK3β instead of a phosphorylation inactivation.
Longer treatment or treatment with another GSK3β inhibitor like andrographolide could give more precise results, especially since pGSK3 seems to decrease instead of increasing with LiCl in these experiments.
An explanation for the contrary results could be the amount of lithium used. A study demonstrated that acute and chronic treatment increased WNT-related genes, with acute treatment administered at a higher concentration of LiCl [86]. The literature also indicated that low-concentration treatment does not change the phosphorylation of Serin 9 or tyrosine 216 [87]. Previous studies also observed a reduction in GSK3β activity without a change in the phosphorylation of GSK3β [88]. Therefore, researchers suggest analysing downstream targets for more knowledge [87].
The difference observed between the cortex and the hippocampus could come from the different lithium uptake. The lithium uptake in juvenile mice is region-specific. After 28 days of treatment, the uptake in the hippocampus was approximately 10 times higher than in the cortex, and during the treatment, the uptake was significantly higher in the hippocampus [89]. Researchers showed that the regional distribution of adult brains differs. While the cortex and the hippocampus contain similar amounts of lithium, the uptake rate in adult mice is not investigated [90]. That suggests that the hippocampus is earlier affected by lithium treatment and that a higher lithium concentration or more extended treatment could lead to changes in the cortex.

Hence, investigating the connection between WNT and mtUPR requires the correct treatment. Further investigation should consider using differentiated cells and extended treatment for mice or treating with another GSK3β inhibitor to prove the connection.
Further research can consider using qPCR to prove that these observations come from an increase in transcription and not in translation. It would increase the understanding of the connection to investigate if WNT activation directly increases mtUPR-related proteins or if it only increases the translation of ATF5, which then activates mtUPR. Therefore, inhibition of ATF5 transcription can show the role of ATF5.
WNT functions during development and leads to the expression of genes related to the cytoskeleton and synaptic activity [33]. New studies indicate that understanding mtUPR and its connections could be beneficial during disease [42], [61]. This field of interactions is still relatively new, and it is unclear if the connection can be bidirectional. Previous research found a connection with the unfolded protein response of the endoplasmic reticulum (erUPR). Researchers observed that the erUPR can decrease the WNT signalling in cancer cells, C. elegans and Zebrafish [91], [92]. In zebrafish and colon cancer cells, malfunction of the ATP synthesis in mitochondria can lead to stress in the endoplasmic reticulum, which downregulates WNT [92]. That indicates that the interaction between WNT and cellular stress pathways is highly complex, and a better understanding could bring new insights into different diseases.

This study suggests a canonical WNT signalling pathway and mtUPR connection in cells. Furthermore, WNT signalling activation in the hippocampus of mice increases mtUPR proteins. The correct lithium concentration is essential for all experiments, and regulation of GSK3β by lithium needs further investigation. Further experiments with other WNT inhibitors, differentiated cells, and longer treatments could lead to more insight and possible targets for Alzheimer's disease.

4 Methods

The exact description of the materials used can be found in the appendix (8.1).

4.1 Bioinformatic promotor analysis

TCF7 and LEF1 are the best-characterised transcription factor families. β-catenin can interact with both families. There are different sequences where these transcription factors can bind. [30]
It is CTTTGAT for TCF7, AAAGATCAAAGG for TCF7L1, AGATCAAAG for TCF7L2 and AAGATCAAAG for LEF1 in humans and CCTTTGAT for LEF1 as well as AAAGATCAAAGG for TCF7 in mouse.[93]
So, the different promotor sequences were looked up at https://www.ensembl.org/index.html. 2000 bp before and 500 bp after the transcription start site were copied, and then https://jaspar.genereg.net/ was used to find sequences within the promotor using a relative profile score threshold of 80 % for each factor for humans and mice.

4.2 Cell culture

4.2.1 SHSY5Y cells

SH-SY5Y cells originate in the SK-N-SH cell line, generated from a bone marrow biopsy in the 1970s [94].

4.2.1.1 Maintenance

Cells were used for experiments within a passage number of five to ten. Cells were fed every 2 to 3 days with Maintenance Medium containing DMEM low glucose, 10 % fetal bovine serum, 2 mM Glutamine and 1 % antibiotics/antimycotic.
The amount of medium used depended on the size of the plate, as noted in Table 4.

Table 4: Plate size and exact numbers
The following tables state the exact numbers used for feeding and seeding cells in different plate sizes.

Size (Area – Diameter)	Seeded cell number	Media used
56.7 cm^2 – 100 mm	400 000	6 mL
21.5 cm^2 – 60 mm	350 000	5 mL
9.5 cm^2 – 35 mm – 6 wells	250 000	2 mL
1.93 cm^2 – 15 mm – 24 wells	5 000	0,5 mL

4.2.1.2 Splitting

Depending on further experiments, the cells were split at 80 % confluency and distributed into different cell culture types. The exact cell numbers added to each dish are noted in Table 4.
For the splitting process, the medium was removed, and the cells were washed two times with 2 mL PBS. For detaching, 1 mL of warm Trypsin was added to 100 mm plates and then incubated for 3 min at 37 °C. The reaction was stopped using 2 mL of medium, and the cells were then transferred to a 15 mL falcon tube. The plate was washed with 3 mL medium to collect all the cells and then centrifuged at 1000 g for 3 min at room temperature (RT). The supernatant was aspirated, and 2 mL medium was added. 10 µL of the suspension and

10 µL Trypan blue were mixed, and a hemocytometer was used to count the cells. The number of cells per mL was calculated, and then the amount of suspension needed to be seeded to get the desired number of cells noted in Table 4 was prepared and added to the plate.

4.2.1.3 Lithium treatment

The numbers of cells mentioned above were treated approximately 2 to 3 days after seeding at around 70 % confluency by discarding the medium and adding fresh medium containing different concentrations of lithium chloride. The cells were then incubated at 37 °C for 1, 6 or 24 hours. The lithium chloride concentrations were 1, 5, 10, 15 and 20 mM to evaluate the correct concentration. Afterwards, 5 and 10 mM were used for 1 and 24h. Cells were treated at around 30 % confluency for the immunofluorescence to investigate single cells.

4.2.1.4 Differentiation

After splitting the cells, the plates were incubated with a maintenance medium until 50 % confluency. Then, the medium was discarded, cells were washed twice with 2 mL 1X PBS, and differentiation medium was added as indicated in Table 4. Cells were incubated at 37 °C for 7 days, and the medium was changed every 3 to 4 days. The differentiation medium contained DMEM low glucose, 1 % fetal bovine serum (FBS), 2 mM Glutamine, 1 % antibiotics and 10 µM retinoic acid. Retinoic acid was added immediately before use from a 5 mM stock solution. Retinoic acid was kept in the freezer and in the dark.

4.3 Animals and experimental procedures

The protocol was created based on Gould 2007 and Xiang 2021 [81], [82]. These experiments used two- to three-month-old C57BL/6J wild-type mice. The mice were maintained in a 12/12 h light/dark cycle at 23°C, fed *ad libitum* with standard chow and sterilised, acidic water. Eight mice per experimental design were divided into two groups of four. The first experiment contained seven intraperitoneal injections every second day with 2,3 mmol of lithium chloride per kg in NaCl saline solution. The second experiment was conducted with 14 daily injections. Four mice were used as a control group and were only injected with 0,9 % NaCl saline solution. The other four mice in the treatment group were injected with 0,9 % NaCl-0,7 M LiCl solution. On day 15, mice were sacrificed after anaesthetized with Isoflurane and decapitated. All materials, including forceps, scissors and tubes, were kept on ice. Tubes for protein extraction were filled with RIPA Buffer and kept on ice afterwards. Tubes for RNA were transferred directly to the -80 °C freezer. The scalp was opened, and the brain dissected. The olfactory bulb and the Cerebellum were discarded. The hippocampus and Cortex were saved in two separate tubes.

4.4 Western Blot

The following Buffers needed to be prepared before the start of the procedure:

- Running Buffer: 25 mM Tris, 192 mM Glycine, 10 % SDS.
- Transfer Buffer: 25 mM Tris, 192 mM Glycine, 20 % Methanol.
- TBS-T: 20 mM Tris, 150 mM NaCl, 0,1 % Tween-20
- Blocking Milk: 5 % fat-free Milk powder in TBS-T.
- Primary Antibodies: 1:1000 dilution with 5 % BSA in TBS-T.
- Secondary Antibodies were diluted 1:5000 in milk.

- Stripping solution: 25 mM glycine. 1 % SDS. pH 2.
- RIPA buffer: 150 mM NaCl, 0,1 % SDS, 1 % Triton X-100, 50 mM Tris, pH 8. Shortly before use, protease inhibitors and phosphatase inhibitors were added.
- Phosphatase inhibitors: 0,05 M NaF and 0,001 M Na_3VO_4
- Sample Buffer: 0,08 M Tris, 2,3 % SDS, 10 % Glycerol, 5 % 2-Mercaptoethanol, 0,006 % Bromophenol Blue.
- Stacking buffer: 1 M Tris, pH 6,8.
- Running buffer: 1,5 M Tris, pH 8,8
- PBS contained 137 mM NaCl, 2,7 mM KCl, 10 mM Na_2HPO_4, 1.8 mM KH_2PO_4

Protein preparation

The Protein extraction was done by discarding the medium and washing it twice with 1 mL cold PBS. The plates could be frozen at that time for no more than 48 hours at -80 °C. Then, 80 µL RIPA buffer was added, and the cells were scrapped using a Digralasky spreader. The plates were incubated for 15 min while shaking. All liquid was then transferred to an Eppendorf tube. The tubes were incubated for 30 min while shaking. It was then centrifuged at 12 000 g and 4 °C for 20 min.

For the mouse hippocampus, 600 µL and the cortex, 800 µL of RIPA buffer were added to the tube containing the tissue. The tissues were homogenised by mechanical force with a plastic mini homogeniser and pipetting. It was then centrifuged at 14 000 rpm and 4 °C for 20 min.

The supernatant was saved in a new tube, and the concentration was quantified using the BCA test according to the manufacturer's instructions. Unused protein was stored at -80 °C. The samples were kept on ice at all times.

Gel preparation

The gels were prepared depending on the size of the proteins of interest. Thereby, 6 to 8 % were used for proteins smaller than 25 kD. While 10 % were used for proteins from 25 to 150 kD and 12 to 15% for bigger than 150 kD

The first step was to prepare the gel stand and fill it with water to test for leakage. Then, the resolving gel was prepared using 5 mL per gel. It was added to the gel stand and hardened with 1 mL of Isopropanol. That was discarded before adding the stacking gel. Before adding the comp, 3 mL per gel was prepared and filled to the top. It was again left to harden and was then stored in a plastic bag with ddH2O at 4 °C.

Gel electrophoresis

The gels were removed from the fridge and returned to the gel stand. Then, it was added to the gel electrophoresis chamber and filled with the running buffer. The chomp was removed, and 20 to 30 µL samples were loaded after heating up for 5 min at 95 °C. It was run at 80 V for 30 min and then turned to 100 V for 1.5 h.

Transfer

The Membrane was soaked in methanol for 3 min and then changed to transfer buffer. Then, the transfer chamber was prepared, and the transfer buffer was added. The black plate, sponge, filter paper, Gel, membrane, filter paper, sponge and red plate were prepared as a sandwich and added to the Transfer box. Then, it was filled up with the transfer buffer. The box in the fridge was filled with ice, and the Transfer box was added. It was then run at 300 A, 300 V for 120 min.

Staining
The membrane was stained using Ponzu red to prove the transfer and to be able to cut the membrane correctly. It was left in Ponzu red for 5 min and then washed with H2O. 1X PBS was used for unstaining. Then, the membrane was blocked with 5 % milk for 1 h. It was washed with TBS-T thrice for 5 min before adding 5 mL of primary antibody. It was incubated overnight at 4 °C. The next day, it was washed thrice for 5 min with TBS-T. Then, 5 mL secondary antibody was used for 1 h at RT. After washing again with TBS-T 3 times for 5 min, the membrane was stored in PBS. Luminizenz was used for analysing the membrane.

Analysing
500µL Peroxidase and 500 µL Luminol-Enhancer were mixed, and the membrane was incubated for 3 min. It was then imaged together with the colouric marker.

Stripping
A stripping step was performed if the membrane needed to be incubated with a second primary antibody. The stripping solution was used two times for 15 min each to remove the secondary antibody, and the restored stripping solution was used for 5 min to remove the primary antibody. It was then washed three times for 5 min with TBS-T. As mentioned, it was again blocked in 5 % Milk and stained.

Quantification
Image J was used to quantify all Western Blot images. The pictures were opened and straightened using Image (Transform → Rotate) if necessary. All bands for analysis were then chosen using the rectangular. Then, all lanes were selected and analysed. The line tool was used to separate the peaks, and they were then measured using the line Wand (tracing) tool. All measurements were copied into an Excel for further analysis.

Statistical Analysis
All measurements were normalised to the housekeeping protein and then normalised to the control. In the case of the analysis of a modified protein, it was also normalised to the total protein concentration. All values were then added to GraphPad for the statistical analysis using a one-way-ANOVA, which was not paired, and each column was compared. A p-value smaller than 0,5 was considered significant. The statistical analysis was always done after three replicates were analysed.

4.5 Statistics

A one-way ANOVA with repeated measurements was used for cells, and for all mouse comparisons, a t-test between controls and treatments was performed.

5 Bibliography

[1] Alzheimer Association, 'Alzheimer's Disease Facts and Figures', Alzheimer's Disease and Dementia. Accessed: Mar. 09, 2023. [Online]. Available: https://www.alz.org/alzheimers-dementia/facts-figures

[2] Alzheimer Europe, 'Prevalence of dementia in Europe', 2019, Accessed: Sep. 21, 2023. [Online]. Available: https://www.alzheimer-europe.org/dementia/prevalence-dementia-europe

[3] OECD and European Union, *Health at a Glance: Europe 2018: State of Health in the EU Cycle*. in Health at a Glance: Europe. OECD, 2018. doi: 10.1787/health_glance_eur-2018-en.

[4] A. S. Coprad-sonepsyn, P. A. Sonepsyn, J. M. Coprad, and R. R. Coprad, 'Enfermedad de Alzheimer y otras en Chile. Propuesta de un Plan Nacional de Alzheimer y otras Demencias'.

[5] D. A. fuer P. Oeffentlichkeitsarbeit, 'Faktenzentrale', DZNE. Accessed: Sep. 21, 2023. [Online]. Available: https://www.dzne.de/aktuelles/hintergrund/faktenzentrale/

[6] 'Population of EUROPE 2018 - PopulationPyramid.net'. Accessed: Sep. 27, 2023. [Online]. Available: https://www.populationpyramid.net/europe/2018/

[7] A. K. Torres *et al.*, 'Synaptic Mitochondria: An Early Target of Amyloid-β and Tau in Alzheimer's Disease', *J. Alzheimers Dis.*, vol. 84, no. 4, pp. 1391–1414, Dec. 2021, doi: 10.3233/JAD-215139.

[8] L. Wu *et al.*, 'Early-Onset Familial Alzheimer's Disease (EOFAD)', *Can. J. Neurol. Sci.*, vol. 39, no. 4, pp. 436–445, Jul. 2012, doi: 10.1017/S0317167100013949.

[9] U. C. Müller, T. Deller, and M. Korte, 'Not just amyloid: physiological functions of the amyloid precursor protein family', *Nat. Rev. Neurosci.*, vol. 18, no. 5, Art. no. 5, May 2017, doi: 10.1038/nrn.2017.29.

[10] A. Tandon and P. Fraser, 'The presenilins', *Genome Biol.*, vol. 3, no. 11, p. reviews3014.1-reviews3014.9, 2002, doi: 10.1186/gb-2002-3-11-reviews3014.

[11] J. Zhao, X. Liu, W. Xia, Y. Zhang, and C. Wang, 'Targeting Amyloidogenic Processing of APP in Alzheimer's Disease', *Front. Mol. Neurosci.*, vol. 13, 2020, Accessed: Nov. 17, 2022. [Online]. Available: https://www.frontiersin.org/articles/10.3389/fnmol.2020.00137

[12] P. Villaseca, P. Cisternas, and N. C. Inestrosa, 'Menopause and development of Alzheimer's disease: Roles of neural glucose metabolism and Wnt signaling', *Front. Endocrinol.*, vol. 13, 2022, Accessed: Sep. 26, 2023. [Online]. Available: https://www.frontiersin.org/articles/10.3389/fendo.2022.1021796

[13] H. Steiner, A. Fukumori, S. Tagami, and M. Okochi, 'Making the final cut: pathogenic amyloid-β peptide generation by γ-secretase', *Cell Stress*, vol. 2, no. 11, pp. 292–310, doi: 10.15698/cst2018.11.162.

[14] Y. Zhang, R. Thompson, H. Zhang, and H. Xu, 'APP processing in Alzheimer's disease', *Mol. Brain*, vol. 4, no. 1, p. 3, Jan. 2011, doi: 10.1186/1756-6606-4-3.

[15] U. Sengupta, A. N. Nilson, and R. Kayed, 'The Role of Amyloid-β Oligomers in Toxicity, Propagation, and Immunotherapy', *EBioMedicine*, vol. 6, pp. 42–49, Apr. 2016, doi: 10.1016/j.ebiom.2016.03.035.

[16] K. Iqbal, F. Liu, C.-X. Gong, and I. Grundke-Iqbal, 'Tau in Alzheimer Disease and Related Tauopathies', *Curr. Alzheimer Res.*, vol. 7, no. 8, pp. 656–664.

[17] A. Mietelska-Porowska, U. Wasik, M. Goras, A. Filipek, and G. Niewiadomska, 'Tau Protein Modifications and Interactions: Their Role in Function and Dysfunction', *Int. J. Mol. Sci.*, vol. 15, no. 3, pp. 4671–4713, Mar. 2014, doi: 10.3390/ijms15034671.

[18] B. W. Doble, S. Patel, G. A. Wood, L. K. Kockeritz, and J. R. Woodgett, 'Functional Redundancy of GSK-3α and GSK-3β in Wnt/β-Catenin Signaling Shown by Using an Allelic Series of Embryonic Stem Cell Lines', *Dev. Cell*, vol. 12, no. 6, pp. 957–971, Jun. 2007, doi: 10.1016/j.devcel.2007.04.001.

[19] J.-Z. Wang and F. Liu, 'Microtubule-associated protein tau in development, degeneration and protection of neurons', *Prog. Neurobiol.*, vol. 85, no. 2, pp. 148–175, Jun. 2008, doi: 10.1016/j.pneurobio.2008.03.002.

[20] C. Jie, V. Treyer, R. Schibli, and L. Mu, 'Tauvid™: The First FDA-Approved PET Tracer for Imaging Tau Pathology in Alzheimer's Disease', *Pharmaceuticals*, vol. 14, p. 110, Jan. 2021, doi: 10.3390/ph14020110.

[21] A. del C. Alonso, I. Grundke-Iqbal, and K. Iqbal, 'Alzheimer's disease hyperphosphorylated tau sequesters normal tau into tangles of filaments and disassembles microtubules', *Nat. Med.*, vol. 2, no. 7, Art. no. 7, Jul. 1996, doi: 10.1038/nm0796-783.

[22] P. W. Baas, A. N. Rao, A. J. Matamoros, and L. Leo, 'Stability properties of neuronal microtubules', *Cytoskelet. Hoboken NJ*, vol. 73, no. 9, pp. 442–460, Sep. 2016, doi: 10.1002/cm.21286.

[23] Y. L. Rao, B. Ganaraja, B. V. Murlimanju, T. Joy, A. Krishnamurthy, and A. Agrawal, 'Hippocampus and its involvement in Alzheimer's disease: a review', *3 Biotech*, vol. 12, no. 2, p. 55, Feb. 2022, doi: 10.1007/s13205-022-03123-4.

[24] Q.-S. Chen, B. L. Kagan, Y. Hirakura, and C.-W. Xie, 'Impairment of hippocampal long-term potentiation by Alzheimer amyloid β-peptides', *J. Neurosci. Res.*, vol. 60, no. 1, pp. 65–72, 2000, doi: 10.1002/(SICI)1097-4547(20000401)60:1<65::AID-JNR7>3.0.CO;2-Q.

[25] W. Fu and J. H. Jhamandas, 'Chapter 20 - Amylin and amylin receptors in Alzheimer's disease', in *Genetics, Neurology, Behavior, and Diet in Dementia*, C. R. Martin and V. R. Preedy, Eds., Academic Press, 2020, pp. 309–324. doi: 10.1016/B978-0-12-815868-5.00020-7.

[26] G. V. De Ferrari *et al.*, 'Activation of Wnt signaling rescues neurodegeneration and behavioral impairments induced by β-amyloid fibrils', *Mol. Psychiatry*, vol. 8, no. 2, Art. no. 2, Feb. 2003, doi: 10.1038/sj.mp.4001208.

[27] S. Tu, S. Okamoto, S. A. Lipton, and H. Xu, 'Oligomeric Aβ-induced synaptic dysfunction in Alzheimer's disease', *Mol. Neurodegener.*, vol. 9, no. 1, p. 48, Nov. 2014, doi: 10.1186/1750-1326-9-48.

[28] C. Tapia-Rojas, P. V. Burgos, and N. C. Inestrosa, 'Inhibition of Wnt signaling induces amyloidogenic processing of amyloid precursor protein and the production and aggregation of Amyloid-β (Aβ)42 peptides', vol. 139, pp. 1175-1191Tapia-Rojas, 2016, doi: 10.1111/jnc.13873.

[29] E. Palomer, J. Buechler, and P. C. Salinas, 'Wnt Signaling Deregulation in the Aging and Alzheimer's Brain', *Front. Cell. Neurosci.*, vol. 13, p. 227, 2019, doi: 10.3389/fncel.2019.00227.

[30] K. M. Cadigan and M. L. Waterman, 'TCF/LEFs and Wnt Signaling in the Nucleus', *Cold Spring Harb. Perspect. Biol.*, vol. 4, no. 11, pp. a007906–a007906, Nov. 2012, doi: 10.1101/cshperspect.a007906.

[31] B. T. MacDonald, K. Tamai, and X. He, 'Wnt/β-catenin signaling: components, mechanisms, and diseases', *Dev. Cell*, vol. 17, no. 1, p. 9, Jul. 2009, doi: 10.1016/j.devcel.2009.06.016.

[32] D. Wawrzak, A. Luyten, K. Lambaerts, and P. Zimmermann, 'Frizzled–PDZ scaffold interactions in the control of Wnt signaling', *Adv. Enzyme Regul.*, vol. 49, no. 1, pp. 98–106, Jan. 2009, doi: 10.1016/j.advenzreg.2009.01.002.

[33] N. C. Inestrosa and L. Varela-Nallar, 'Wnt signaling in the nervous system and in Alzheimer's disease', *J. Mol. Cell Biol.*, vol. 6, no. 1, pp. 64–74, Feb. 2014, doi: 10.1093/jmcb/mjt051.
[34] M. Sharma and K. Pruitt, 'Wnt Pathway: An Integral Hub for Developmental and Oncogenic Signaling Networks', *Int. J. Mol. Sci.*, vol. 21, no. 21, Art. no. 21, Jan. 2020, doi: 10.3390/ijms21218018.
[35] M. E. Snitow, R. S. Bhansali, and P. S. Klein, 'Lithium and Therapeutic Targeting of GSK-3', *Cells*, vol. 10, no. 2, p. 255, Jan. 2021, doi: 10.3390/cells10020255.
[36] W. Zhang, R. A. Stetler, and J. Chen, 'Chapter 55 - Akt-GSK3β Pro-survival Signaling Pathway in Cerebral Ischemic Injury', in *Primer on Cerebrovascular Diseases (Second Edition)*, L. R. Caplan, J. Biller, M. C. Leary, E. H. Lo, A. J. Thomas, M. Yenari, and J. H. Zhang, Eds., San Diego: Academic Press, 2017, pp. 269–272. doi: 10.1016/B978-0-12-803058-5.00055-2.
[37] L. F. Ng *et al.*, 'WNT Signaling in Disease', *Cells*, vol. 8, no. 8, Art. no. 8, Aug. 2019, doi: 10.3390/cells8080826.
[38] J. L. Stamos and W. I. Weis, 'The β-Catenin Destruction Complex', *Cold Spring Harb. Perspect. Biol.*, vol. 5, no. 1, p. a007898, Jan. 2013, doi: 10.1101/cshperspect.a007898.
[39] W. Cerpa, G. G. Farías, J. A. Godoy, M. Fuenzalida, C. Bonansco, and N. C. Inestrosa, 'Wnt-5a occludes Aβ oligomer-induced depression of glutamatergic transmission in hippocampal neurons', *Mol. Neurodegener.*, vol. 5, p. 3, Jan. 2010, doi: 10.1186/1750-1326-5-3.
[40] NCBI, 'DKK1 dickkopf WNT signaling pathway inhibitor 1 [Homo sapiens (human)]'. Jul. 09, 2023. [Online]. Available: https://www.ncbi.nlm.nih.gov/gene/22943
[41] F. Hadi, H. Akrami, K. Shahpasand, and M. R. Fattahi, 'Wnt signalling pathway and tau phosphorylation: A comprehensive study on known connections', *Cell Biochem. Funct.*, vol. 38, no. 6, pp. 686–694, 2020, doi: 10.1002/cbf.3530.
[42] Q. Zhang *et al.*, 'The Mitochondrial Unfolded Protein Response Is Mediated Cell-Non-autonomously by Retromer-Dependent Wnt Signaling', *Cell*, vol. 174, no. 4, pp. 870-883.e17, Aug. 2018, doi: 10.1016/j.cell.2018.06.029.
[43] N. S. Anderson and C. M. Haynes, 'Folding the Mitochondrial UPR into the Integrated Stress Response', *Trends Cell Biol.*, vol. 30, no. 6, pp. 428–439, Jun. 2020, doi: 10.1016/j.tcb.2020.03.001.
[44] V. Sorrentino *et al.*, 'Enhancing mitochondrial proteostasis reduces amyloid-β proteotoxicity', *Nature*, vol. 552, no. 7684, Art. no. 7684, Dec. 2017, doi: 10.1038/nature25143.
[45] R. H. Swerdlow, J. M. Burns, and S. M. Khan, 'The Alzheimer's Disease Mitochondrial Cascade Hypothesis', *J. Alzheimers Dis.*, vol. 20, no. s2, pp. S265–S279, Jun. 2010, doi: 10.3233/JAD-2010-100339.
[46] C. M. Haynes, K. Petrova, C. Benedetti, Y. Yang, and D. Ron, 'ClpP Mediates Activation of a Mitochondrial Unfolded Protein Response in C. elegans', *Dev. Cell*, vol. 13, no. 4, pp. 467–480, Oct. 2007, doi: 10.1016/j.devcel.2007.07.016.
[47] T. Arnould, S. Michel, and P. Renard, 'Mitochondria Retrograde Signaling and the UPRmt: Where Are We in Mammals?', *Int. J. Mol. Sci.*, vol. 16, no. 8, Art. no. 8, Aug. 2015, doi: 10.3390/ijms160818224.
[48] T. Ji *et al.*, 'Does perturbation in the mitochondrial protein folding pave the way for neurodegeneration diseases?', *Ageing Res. Rev.*, vol. 57, p. 100997, Jan. 2020, doi: 10.1016/j.arr.2019.100997.

[49] T. Y. Li *et al.*, 'The transcriptional coactivator CBP/p300 is an evolutionarily conserved node that promotes longevity in response to mitochondrial stress', *Nat. Ageing*, vol. 1, no. 2, pp. 165–178, Feb. 2021, doi: 10.1038/s43587-020-00025-z.
[50] A. Mottis, V. Jovaisaite, and J. Auwerx, 'The mitochondrial unfolded protein response in mammalian physiology', *Mamm. Genome*, vol. 25, no. 9, pp. 424–433, Oct. 2014, doi: 10.1007/s00335-014-9525-z.
[51] I. Smyrnias, 'The mitochondrial unfolded protein response and its diverse roles in cellular stress', *Int. J. Biochem. Cell Biol.*, vol. 133, p. 105934, Apr. 2021, doi: 10.1016/j.biocel.2021.105934.
[52] K. Pakos-Zebrucka, I. Koryga, K. Mnich, M. Ljujic, A. Samali, and A. M. Gorman, 'The integrated stress response', *EMBO Rep.*, vol. 17, no. 10, pp. 1374–1395, Oct. 2016, doi: 10.15252/embr.201642195.
[53] Q. Yang *et al.*, 'LONP-1 and ATFS-1 sustain deleterious heteroplasmy by promoting mtDNA replication in dysfunctional mitochondria', *Nat. Cell Biol.*, vol. 24, no. 2, pp. 181–193, Feb. 2022, doi: 10.1038/s41556-021-00840-5.
[54] X. Guo *et al.*, 'Mitochondrial stress is relayed to the cytosol by an OMA1-DELE1-HRI pathway', *Nature*, vol. 579, no. 7799, pp. 427–432, Mar. 2020, doi: 10.1038/s41586-020-2078-2.
[55] Z.-H. Sheng and Q. Cai, 'Mitochondrial transport in neurons: impact on synaptic homeostasis and neurodegeneration', *Nat. Rev. Neurosci.*, vol. 13, no. 2, pp. 77–93, Jan. 2012, doi: 10.1038/nrn3156.
[56] C. Jara, A. Aránguiz, W. Cerpa, C. Tapia-Rojas, and R. A. Quintanilla, 'Genetic ablation of tau improves mitochondrial function and cognitive abilities in the hippocampus', *Redox Biol.*, vol. 18, pp. 279–294, Jul. 2018, doi: 10.1016/j.redox.2018.07.010.
[57] M. A. Olesen, A. K. Torres, C. Jara, M. P. Murphy, and C. Tapia-Rojas, 'Premature synaptic mitochondrial dysfunction in the hippocampus during aging contributes to memory loss', *Redox Biol.*, vol. 34, p. 101558, Jul. 2020, doi: 10.1016/j.redox.2020.101558.
[58] V. Arnaboldi and R. Kishore, 'hsp-6 (gene) - WormBase : Nematode Information Resource'. Accessed: Feb. 25, 2023. [Online]. Available: https://wormbase.org/species/c_elegans/gene/WBGene00002010#0-9f-10
[59] M. Lefers, 'cell autonomous definition'. Accessed: Jul. 27, 2023. [Online]. Available: https://groups.molbiosci.northwestern.edu/holmgren/Glossary/Definitions/Def-C/cell_autonomous.html
[60] 'HomoloGene - NCBI'. Accessed: Oct. 06, 2023. [Online]. Available: https://www.ncbi.nlm.nih.gov/homologene?term=hsp-6&cmd=Search
[61] P. X. Chen, L. Zhang, D. Chen, and Y. Tian, 'Mitochondrial stress and aging: Lessons from C. elegans', *Semin. Cell Dev. Biol.*, Feb. 2023, doi: 10.1016/j.semcdb.2023.02.010.
[62] A. Jämsä, K. Hasslund, R. F. Cowburn, A. Bäckström, and M. Vasänge, 'The retinoic acid and brain-derived neurotrophic factor differentiated SH-SY5Y cell line as a model for Alzheimer's disease-like tau phosphorylation', *Biochem. Biophys. Res. Commun.*, vol. 319, no. 3, pp. 993–1000, Jul. 2004, doi: 10.1016/j.bbrc.2004.05.075.
[63] O. C. Ioghen, L. C. Ceafalan, and B. O. Popescu, 'SH-SY5Y Cell Line In Vitro Models for Parkinson Disease Research—Old Practice for New Trends', *J. Integr. Neurosci.*, vol. 22, no. 1, Art. no. 1, Jan. 2023, doi: 10.31083/j.jin2201020.
[64] M. Sedighi, T. Baluchnejadmojarad, and M. Roghani, 'Linagliptin Protects Human SH-SY5Y Neuroblastoma Cells against Amyloid-β Cytotoxicity via the Activation of

Wnt1 and Suppression of IL-6 Release', *Iran. Biomed. J.*, vol. 25, no. 5, pp. 343–348, Sep. 2021, doi: 10.52547/ibj.25.5.343.
[65] M. Zhang *et al.*, 'Differentially expressed long-chain noncoding RNAs in human neuroblastoma cell line (SH-SY5Y): Alzheimer's disease cell model', *J. Toxicol. Environ. Health A*, vol. 82, no. 19, pp. 1052–1060, Oct. 2019, doi: 10.1080/15287394.2019.1687183.
[66] 'What is a mouse model?', The Jackson Laboratory. Accessed: Apr. 22, 2024. [Online]. Available: https://www.jax.org/why-the-mouse/model
[67] C. Volkmann, T. Bschor, and S. Köhler, 'Lithium Treatment Over the Lifespan in Bipolar Disorders', *Front. Psychiatry*, vol. 11, p. 377, May 2020, doi: 10.3389/fpsyt.2020.00377.
[68] 'Ensembl genome browser 111'. Accessed: Mar. 26, 2024. [Online]. Available: https://www.ensembl.org/index.html
[69] M. Martinez, V. I. Torres, C. P. Vio, and N. C. Inestrosa, 'Canonical Wnt Signaling Modulates the Expression of Pre- and Postsynaptic Components in Different Temporal Patterns', *Mol. Neurobiol.*, vol. 57, no. 3, pp. 1389–1404, Mar. 2020, doi: 10.1007/s12035-019-01785-5.
[70] C. Hödar *et al.*, 'Genome-wide identification of new Wnt/β-catenin target genes in the human genome using CART method', *BMC Genomics*, vol. 11, no. 1, p. 348, Jun. 2010, doi: 10.1186/1471-2164-11-348.
[71] R. S. Jope, 'Lithium and GSK-3: one inhibitor, two inhibitory actions, multiple outcomes', *Trends Pharmacol. Sci.*, vol. 24, no. 9, pp. 441–443, Sep. 2003, doi: 10.1016/S0165-6147(03)00206-2.
[72] M. S. Arrázola *et al.*, 'Calcium/calmodulin-dependent protein kinase type IV is a target gene of the Wnt/β-catenin signaling pathway', *J. Cell. Physiol.*, vol. 221, no. 3, pp. 658–667, 2009, doi: 10.1002/jcp.21902.
[73] K. B. Magalingam, A. K. Radhakrishnan, S. D. Somanath, S. Md, and N. Haleagrahara, 'Influence of serum concentration in retinoic acid and phorbol ester induced differentiation of SH-SY5Y human neuroblastoma cell line', *Mol. Biol. Rep.*, vol. 47, no. 11, pp. 8775–8788, Nov. 2020, doi: 10.1007/s11033-020-05925-2.
[74] J. A. Korecka *et al.*, 'Phenotypic Characterization of Retinoic Acid Differentiated SH-SY5Y Cells by Transcriptional Profiling', *PLOS ONE*, vol. 8, no. 5, p. e63862, May 2013, doi: 10.1371/journal.pone.0063862.
[75] Z. Xun *et al.*, 'Retinoic acid-induced differentiation increases the rate of oxygen consumption and enhances the spare respiratory capacity of mitochondria in SH-SY5Y cells', *Mech. Ageing Dev.*, vol. 133, no. 4, pp. 176–185, Apr. 2012, doi: 10.1016/j.mad.2012.01.008.
[76] 'Quantitative Characterization of Phenotypical Markers After Diffe...: Ingenta Connect'. Accessed: Nov. 27, 2023. [Online]. Available: https://www.ingentaconnect.com/content/ben/cnsnddt/2020/00000019/00000008/art00009
[77] J. Kovalevich and D. Langford, 'Considerations for the Use of SH-SY5Y Neuroblastoma Cells in Neurobiology', in *Neuronal Cell Culture: Methods and Protocols*, S. Amini and M. K. White, Eds., in Methods in Molecular Biology. , Totowa, NJ: Humana Press, 2013, pp. 9–21. doi: 10.1007/978-1-62703-640-5_2.
[78] D. Simón *et al.*, 'Pharmacological inhibition of GSK-3 is not strictly correlated with a decrease in tyrosine phosphorylation of residues 216/279', *J. Neurosci. Res.*, vol. 86, no. 3, pp. 668–674, 2008, doi: 10.1002/jnr.21523.
[79] M. Şahin, G. Öncü, M. A. Yılmaz, D. Özkan, and H. Saybaşılı, 'Transformation of SH-SY5Y cell line into neuron-like cells: Investigation of electrophysiological and

biomechanical changes', *Neurosci. Lett.*, vol. 745, p. 135628, Feb. 2021, doi: 10.1016/j.neulet.2021.135628.
[80] J. R. Murillo, L. Goto-Silva, A. Sánchez, F. C. S. Nogueira, G. B. Domont, and M. Junqueira, 'Quantitative proteomic analysis identifies proteins and pathways related to neuronal development in differentiated SH-SY5Y neuroblastoma cells', *EuPA Open Proteomics*, vol. 16, pp. 1–11, Sep. 2017, doi: 10.1016/j.euprot.2017.06.001.
[81] J. Xiang *et al.*, 'LiCl attenuates impaired learning and memory of APP/PS1 mice, which in mechanism involves α7 nAChRs and Wnt/β-catenin pathway', *J. Cell. Mol. Med.*, vol. 25, no. 22, pp. 10698–10710, 2021, doi: 10.1111/jcmm.17006.
[82] T. D. Gould, K. C. O'Donnell, A. M. Picchini, and H. K. Manji, 'Strain Differences in Lithium Attenuation of d-Amphetamine-Induced Hyperlocomotion: A Mouse Model for the Genetics of Clinical Response to Lithium', *Neuropsychopharmacology*, vol. 32, no. 6, Art. no. 6, Jun. 2007, doi: 10.1038/sj.npp.1301254.
[83] N. Kurgan *et al.*, 'Low dose lithium supplementation activates Wnt/β-catenin signalling and increases bone OPG/RANKL ratio in mice', *Biochem. Biophys. Res. Commun.*, vol. 511, no. 2, pp. 394–397, Apr. 2019, doi: 10.1016/j.bbrc.2019.02.066.
[84] Z. Yu, J. Li, Z. Ge, X. Dang, and K. Wang, 'Lithium prevents rat steroid-related osteonecrosis of the femoral head by β-catenin activation | Endocrine', 2015, Accessed: Dec. 18, 2023. [Online]. Available: https://link.springer.com/article/10.1007/s12020-015-0747-y
[85] A. Noël, L. Barrier, F. Rinaldi, C. Hubert, B. Fauconneau, and S. Ingrand, 'Lithium chloride and staurosporine potentiate the accumulation of phosphorylated glycogen synthase kinase 3β/Tyr216, resulting in glycogen synthase kinase 3β activation in SH-SY5Y human neuroblastoma cell lines', *J. Neurosci. Res.*, vol. 89, no. 5, pp. 755–763, 2011, doi: 10.1002/jnr.22587.
[86] V. J. De-Paula *et al.*, 'Acute and chronic lithium treatment increases Wnt/β-catenin transcripts in cortical and hippocampal tissue at therapeutic concentrations in mice', *Metab. Brain Dis.*, vol. 36, no. 1, pp. 193–197, Jan. 2021, doi: 10.1007/s11011-020-00638-8.
[87] R. K. Fenech, C. R. Ryan, B. Roy, V. A. Fajardo, and R. E. K. MacPherson, 'GSK3 Activity is Decreased in The Hippocampus of Male Mice Supplemented with Low-Dose Lithium in Drinking Water', *FASEB J.*, vol. 34, no. S1, pp. 1–1, 2020, doi: 10.1096/fasebj.2020.34.s1.02945.
[88] R. K. Fenech *et al.*, 'Low-Dose Lithium Supplementation Influences GSK3β Activity in a Brain Region Specific Manner in C57BL6 Male Mice', *J. Alzheimers Dis.*, vol. 91, no. 2, pp. 615–626, Jan. 2023, doi: 10.3233/JAD-220813.
[89] G. Zanni *et al.*, 'Lithium Accumulates in Neurogenic Brain Regions as Revealed by High Resolution Ion Imaging', *Sci. Rep.*, vol. 7, p. 40726, Jan. 2017, doi: 10.1038/srep40726.
[90] M. Thellier, C. Heurteaux, and J.-C. Wissocq, 'Quantitative study of the distribution of lithium in the mouse brain for various doses of lithium given to the animal', *Brain Res.*, vol. 199, no. 1, pp. 175–196, Oct. 1980, doi: 10.1016/0006-8993(80)90239-5.
[91] M. Siri, S. V. Hosseini, S. Dastghaib, and P. Mokarram, 'Crosstalk Between ER Stress, Unfolded Protein Response (UPR) and Wnt Signaling Pathway in Cancer', *Ann. Colorectal Res.*, vol. 8, no. 1, Mar. 2020, doi: 10.30476/acrr.2020.46538.
[92] R. Costa *et al.*, 'Impaired Mitochondrial ATP Production Downregulates Wnt Signaling via ER Stress Induction', *Cell Rep.*, vol. 28, no. 8, pp. 1949-1960.e6, Aug. 2019, doi: 10.1016/j.celrep.2019.07.050.

[93] ‘JASPAR: An open-access database of transcription factor binding profiles’. Accessed: Mar. 13, 2023. [Online]. Available: http://jaspar.genereg.net

[94] H. XIE, L. HU, and G. LI, ‘SH-SY5Y human neuroblastoma cell line: in vitro cell model of dopaminergic neurons in Parkinson’s disease’, *Chin. Med. J. (Engl.)*, vol. 123, no. 08, pp. 1086–1092, Apr. 2010, doi: 10.3760/cma.j.issn.0366-6999.2010.08.021.

6 List of Figures

Figure 1: Dementia and Alzheimer's cases today and in the future The graph shows dementia and Alzheimer's cases in percentages related to the region's population. The population prediction comes from the website populationpyramid.net [6]. It displays the increase in AD cases predicted for 2050. 7
Figure 2: The two pathways of APP processing forming the toxic and non-toxic product The figure shows the processing of APP by α, β and γ-secretase. It displays the non-amyloidogenic way on the right side and the amyloidogenic one on the left, leading to the harmful Aβ. Inspiration comes from the figures from Yun-wu Zhang et al. l.[14] and Jing Zaho et al. l.[11]..... 8
Figure 3: The canonical WNT pathway and its key players This figure shows the different players in the canonical WNT pathway in the absence and presence of WNT ligands. It is inspired by figures seen in papers [34], [37], [38] and created using biorender. On the left side is the pathway displayed in the absence of WNT, where the destruction of complex phosphorylated β-catenin leads to proteasome degradation after ubiquitination by β-TrCP. On the right side, the WNT ligand binds to Frizzled and LRP, inhibiting the destruction complex, the translocation of β-catenin, and the increase in gene transcription. 11
Figure 4: Direct and Indirect Inhibition of GSK3β by Lithium chloride The figure above shows how lithium can inhibit GSK3β. It, therefore, can mimic the WNT pathway leading to an allosteric change or the PI3K-Akt pathway leading to its phosphorylation. It is inspired by [35] and created using biorender. 11
Figure 5: The mtUPR pathway and its key players increase gene transcription in C. elegans and mammals The above figure shows the mtUPR in mammals and C. elegans. It also displays the differences and open questions. This figure is inspired by the papers [48] and [50] and created with PowerPoint and servier medical art graphs. The left side displays the pathway in C. elegans. It shows the leading players in degradation, like Lonp1 and ClpP. ATFS-1 translocates into healthy mitochondria and to the nucleus during mtUPR. ATFS-1 then interacts with UBL-5 and DVE-1 to increase the transcription. The right side shows the mammalian pathway. The pathway is similar to C. elegans. However, the protease Oma1 in the inner mitochondrial membrane is essential, and ATF5 is responsible for protein transcription, along with the IRS proteins ATF4 and CHOP. 15
Figure 6: Aβ and tau, as well as the connection with WNT and mtUPR The figure above visualises the interconnection between Alzheimer-related changes and mitochondrial impairment. It is inspired by [45] and created using biorender. 16
Figure 7: SHSY5Y cells with 1-hour treatment in 5 and 10 mM indicate WNT activation The plots show the increase and decrease in the WNT protein concentration for 0-15 mM LiCl. For all proteins, GAPDH functions as the Housekeeping. The Number of independent experiments (N) is 3. Statistical analysis was a one-way ANOVA. A, B, and C show the plots of the WNT proteins and GAPDH as housekeeping. D is the Graph for CamK IV, E for pGSK3, F for β-catenin and G for Axin2. pGSK3, β-catenin and Axin2 seem to increase. However, none of the results are significant. 20
Figure 8: Morphology change of SHSY5Y cells from alive to dead The figure shows on the left side alive SHSY5Y cells and on the right side dead ones. This morphology change helped distinguish and exclude dead cells from future experiments. Dead cells decreased in size and lost all processes. Both pictures display the cells with a 10X magnification. ... 20
Figure 9: SHSY5Y cells with 6-hour treatment indicating no WNT activation and a high variability The plots show the increase and decrease in the WNT protein concentration for 0-15 mM LiCl. For all proteins, GAPDH functions as the Housekeeping. N is 3. Statistical

analysis was a one-way ANOVA. A, B, and C show the plots of the WNT proteins and GAPDH as housekeeping. D is the Graph for CamK IV, E for pGSK3, F for β-catenin and G for Axin2. Only pGKS3 shows an increase. All other proteins are not changing or decreasing. None of the results were significant. 21
Figure 10: 1, 5 and 10 mM LiCl treatment in SHSY5Y cells with 24-hour treatment indicate WNT activation The plots show the increase and decrease in the WNT protein concentration for 0-15 mM LiCl. For all proteins, GAPDH functions as the Housekeeping. N is 3. Statistical analysis was a one-way ANOVA. A, B, and C show the plots of the WNT proteins and GAPDH as housekeeping. D is the Graph for CamK IV, E for pGSK3, F for β-catenin and G for Axin2. All proteins suggest an increase; Axin2 showed the slightest increase, and no protein was significant. 22
Figure 11: No differentiation, but a phenotypical change occurred in retinoic acid-treated SHSY5Y cells A and B show the plots of the neurogenic and dopaminergic markers with their housekeeping GAPDH. C displays the graph for dopaminergic markers, and D the graphs for neurogenic markers. N is 2, and no statistical evaluation was possible. 23
Figure 12: Morphology change of cells treated with different retinoic acid concentrations The figure above shows the five treatments with retinoic acid. The cells received 0 to 20 µM of retinoic acid for 7 days. All pictures display the cells with a 20X magnification. 24
Figure 13: The experiments showed a non-significant increase in WNT and mtUPR protein levels in 1-hour LiCl treatment Cells received 0 mM, 5 mM and 10 mM LiCl for 1 hour. * Means having a p-value below 0,05 in a one-way ANOVA. A shows the plots of the mitochondrial proteins, B for WNT proteins and C for mtUPR proteins. D displays the graphs for mitochondrial proteins, E for WNT proteins and F for mtUPR proteins. N is 5. 26
Figure 14: Activation of the WNT pathway indicated increased mtUPR protein levels with 24-hour LiCl treatment Cells received 0 mM, 5 mM and 10 mM LiCl for 24 hours. The results indicate an increase of WNT and mtUPR proteins, but only pGSK3 and Lonp1 increased significantly. * Means having a p-value below 0,05 in a one-way ANOVA. A shows the plots of the mitochondrial proteins, B for WNT proteins and C for mtUPR proteins. D displays the graphs for mitochondrial proteins, E for WNT proteins and F for mtUPR proteins. N is 5..... 27
Figure 15: Morphology of cells treated with different LiCL concentrations for 1 and 24 hours The upper lane shows cells treated for one hour, while the lower lane shows pictures of 24-hour treated cells. All pictures display cells with 10X magnification. 28
Figure 16: Every second-day treated Cortex samples show no WNT activation The figure above shows the plots of the WNT, mitochondrial, and mtUPR protein measured in the Cortex samples on the left side and the graphs on the right side. A, B and C are the plots of mitochondrial, WNT and mtUPR proteins and their housekeeping. D shows the analysis of the mitochondrial proteins, while E displays the WNT proteins, and F the mtUPR proteins. * means having a p-value below 0,05. In all mice experiments, the statistical analysis was a t-test. N is 4. 30
Figure 17: Every second-day treated Hippocampus samples do not prove WNT activation The figure above shows the plots of the WNT, mtUPR, and mitochondrial protein measured in the hippocampus samples on the left side and the graphs on the right side. A, B, C and D are the plots of mitochondrial, WNT and mtUPR proteins and their housekeeping. E shows the analysis of the mitochondrial proteins, while F displays the WNT proteins, and G the mtUPR proteins. * means having a p-value below 0,05. In all mice experiments, the statistical analysis was a t-test. N is 4. 31

Figure 18: Cortex samples of everyday treatment do not prove WNT activation The figure above shows the plots of the WNT, mtUPR, and mitochondrial protein measured in the Cortex samples on the left side and the graphs on the right side. A, B and C are the plots of mitochondrial, WNT and mtUPR proteins and their housekeeping. D shows the analysis of the mitochondrial proteins, while E displays the WNT proteins, and F the mtUPR proteins. * means having a p-value below 0,05. In all mice experiments, the statistical analysis was a t-test. N is 4. 32
Figure 19: In everyday treated Hippocampus, WNT activation increased mtUPR proteins The figure above shows the plots of the WNT, mtUPR, and mitochondrial protein measured in the hippocampus samples on the left side and the graphs on the right side. B-catenin and CamK IV increased significantly, indicating the activation of the WNT pathway. Except for Hsp60 mtUPR, proteins significantly increased in the WNT active samples. A, B and C are the plots of mitochondrial, WNT and mtUPR proteins and their housekeeping. D shows the analysis of the mitochondrial proteins, while E displays the WNT proteins, and F the mtUPR proteins. * means having a p-value below 0,05. In all mice experiments, the statistical analysis was a t-test. N is 4. 33
Figure 20: Localisation of ATF5 in LiCl-treated SHSY5Y cells Cells received staining with ATF5 antibody (red), Tom20 antibody (green) and Hoesch (blue). The upper lane shows cells treated with 5 mM, and the lower lane 10 mM LiCl. The magnification of the pictures is 20X. 51
Figure 21: Localisation of β-catenin in LiCl-treated SHSY5Y cells The figure shows cells treated with 0 mM of LiCl on the left, 5 mM in the middle and 10 mM on the right. The nucleus does not display β-catenin signals. The cells received staining with Hoesch (blue) and β-catenin antibody (red). The magnification of the pictures is 40X. 51

7 List of tables

Table 1: Shows the different factors in mtUPR It highlights the difference between mammals and C. elegans [49]. 15
Table 2: Number of possible binding sites of LEF and TCF per promotor in humans The table shows how often Jasper found a specific sequence for binding the transcription factors (LEF1, TCF7, TCF7L1 and TCF7L2) in a specific human promotor. Sequences of interest had a relative profile score threshold of 80% or more. 18
Table 3: Number of possible binding sites of LEF and TCF per promotor in mouse The table shows how often Jasper found a specific sequence for binding the transcription factors (LEF1 and TCF7) in a specific mouse promoter. Sequences of interest had a relative profile score threshold of 80% or more. 18
Table 4: Plate size and exact numbers The following tables state the exact numbers used for feeding and seeding cells in different plate sizes. 37
Table 5: Primary Antibodies All used primary antibodies, origin and concentration. IF stands for Immunofluorescence 54
Table 6: Secondary Antibodies All used secondary antibodies, origin and concentration. 56

8 Additional information

8.1 Example pictures of Immunohistochemistry experiments

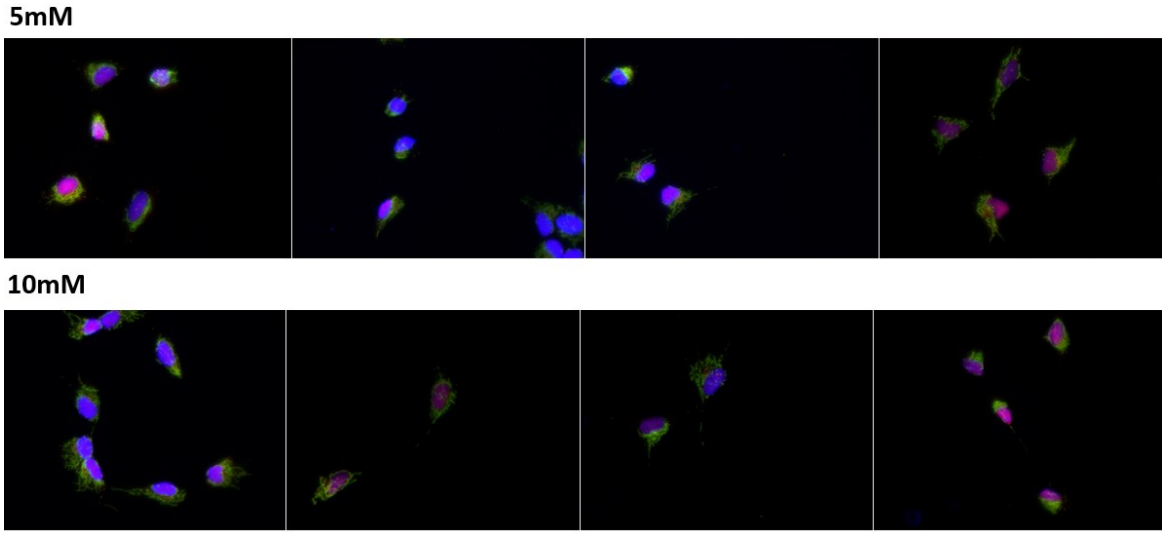

Figure 20: Localisation of ATF5 in LiCl-treated SHSY5Y cells
Cells received staining with ATF5 antibody (red), Tom20 antibody (green) and Hoesch (blue). The upper lane shows cells treated with 5 mM, and the lower lane 10 mM LiCl. The magnification of the pictures is 20X.

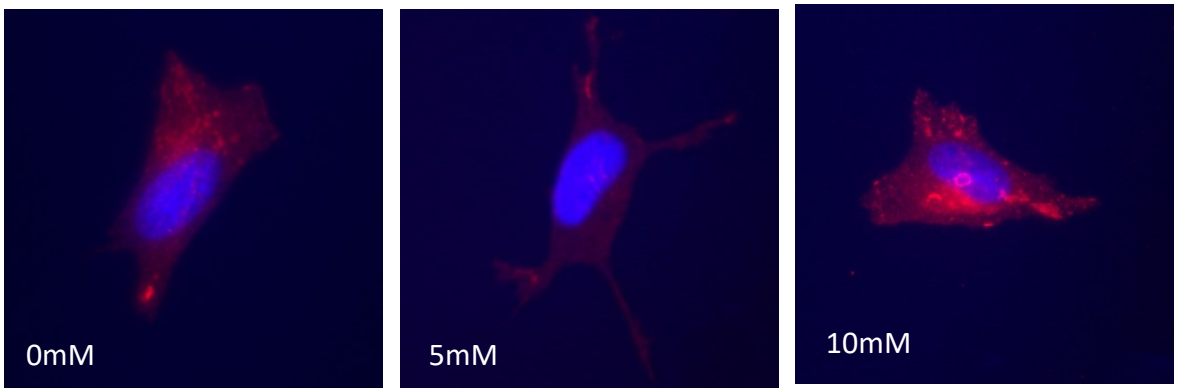

Figure 21: Localisation of β-catenin in LiCl-treated SHSY5Y cells
The figure shows cells treated with 0 mM of LiCl on the left, 5 mM in the middle and 10 mM on the right. The nucleus does not display β-catenin signals. The cells received staining with Hoesch (blue) and β-catenin antibody (red). The magnification of the pictures is 40X.

8.2 Method: Immunofluorescence

Staining

Treated cells were washed three times for three minutes with 500 µL PBS. 4 % PFA was used for one hour to fix the cells at RT while shaking. After that, they were washed again. 500 µL PBS-triton 100X 0,2 % were used for 15 minutes to permeabilise the cells at RT, shaking. They were then blocked using BSA 3 % in PBS-triton 100X 0,2 % for 1 hour at RT, shaking. The lid of the plate is covered in Parafilm, and a drop of 15 µL primary antibody is added to the Parafilm. The coverslip was then removed from the well using a needle and a forceps and was laid inverted onto the drop. The covers were incubated with primary antibodies O.N. at 4 °C in a humidity chamber. Primary and secondary antibodies are diluted 1:200 or 1:100 in the blocking solution.
On the next day, covers were removed from the lid and put back in the wells. They were washed with PBS. The process for the primary antibodies was repeated using the secondary antibodies. From this step, the protocol is continued without light. The secondary antibody was incubated for one hour at RT. The covers were again washed with PBS. It was then

incubated for 5 min with 500 µL Hoesch 1:10000 diluted in PBS. Covers are washed two times, three minutes with PBS and one time five minutes with ddH_2O. Slides were prepared by adding tape and labelling the end of the slide. Then, 5 µL of mounting medium was added, and the covers were added inverted. It was tried for at least three hours, and the edges were sealed with nail polish. The slides were stored at 4 °C.

Imaging
The computer was turned on, and the Mshot Image Analysis system was opened. The number of the lamp, name, date and time were noted, and then the lamp was turned on. The imaging system was started, and the gain and exposure time were set. Then, 15 to 20 cells per condition were imaged and saved as TIF files.

Analysis
A Python program was used to analyse the pictures. The author wrote the program, and the values were compared to those generated using Fiji, the standard method for analysing immunofluorescence. The CTCF value was compared by dividing the Fiji value by the Python value to ensure that the exact behaviour of the results is shown in Python and Fiji. This procedure was done for eight cells in two different pictures, and the difference factor was around 21,000 for all values. This means that a cell with a certain intensity has 21 000 times less intensity in Python, but since that is the case for all cells and no absolute values are compared, the Python program shows the same behaviour as the results. The program is noted in section 8.4, Python source code. The program generated the Area (number of pixels), Mean (Mean grey value = integrated Density/Area), Integrated Density (sum of the mean of intensity in red, green, and blue of all pixels) and the CTCF value (Integrated Density – (Area*Mean of Mean grey value from the background)).
Only the intensity of the red pixels was used, and the pixels were divided into three groups. The background with all pixels under the threshold of 23, the cell with all pixels over 23 without the blue channel staining the nucleus being over 23 and the nucleus with red and blue being over the threshold.
The pictures were prepared for Python using Fiji. The channels were split, the cells were chosen using the freehand tool and the outside was cleared so that only one cell was displayed. That was repeated with all the cells. The positions were saved in the ROI manager, and the process was repeated in the blue channel. Ultimately, all cells were chosen and cleared in red and blue channels to create the background picture.

8.3 Materials

- Pipettes: Corning® Lambda™ Plus Starter Kit, Product Number4069
  25 mL: Costar Stripette 4489
  10 mL: Winkler 12082020
  5 mL: Winkler 99051
- Centrifugation Tubes:
  50 mL: Cornig 430291 or EDLAB 220510
  25mL: EDLAB 210630
- Table centrifuge: DLAB, D1008
- Centrifuge for Eppendorf tubes (1 and 2 mL): Eppendorf Centrifuge 5424R
- Centrifuge for falcons (15 and 50 mL): Eppendorf Centrifuge 5810R
- Excel and Word, Microsoft 365, Version 2303
- Google Scholar, https://scholar.google.at/
- Python: Python 3.8.10 64-bit

- Spyder: Spyder IDE 5.4.1.

8.3.1 Western Blot

- Power supply: Ms major Science, Mini Pro 300V Power Supply, MINI-300
- Luminizenz analyser: Luminizenz Image analyser, ImageQuant LAS500, Codenum 29-0050-63
- Plate reader: Tecan Austria GmbH, Infinite 200 Pro, REF: 30050303, SN 1087003804; Software I control, Infinite Pro 200, Version 3.9.1.0
- Acrylamide Mix: Winkler, BM0100, LOT 20202080
- SDS: Winkler, BM-1650, LOT J1038270
- Ammonium persulfate: Winkler, BM0250, LOT k504100401
- Temed: Winkler, BM1970, LOT NA565970
- Isopropanol: Winkler, LOT C16D14007
- Methanol: Winkler, LOT C011986
- Tris: Winkler, BM-2000, LOT S0002
- Glycine: Winkler, BM-0820, LOT 1641.012320A
- Milk powder: Nestle Svelty Descremada 800g
- Tween-20: Winkler, BM2031, LOT 64312072018
- BSA (Bovin serum albumin) for Antibodies: Winkler BM0150, LOT H190111,
- Luminizenz Kit:
  1. Westar Sun LOT MID08A-FB-3
  2. Westar Antares LOT OH19A-LB-1
  3. Westar Supernova LOT NM19A-LB-2
  4. GenScript LumiSensor LOT L0121401
- BCA quantification:
  1. Thermo Scientific, Micro BCA Protein Assay Kit, 23235, LOT: UL292704
  2. Novagen, BCA Protein Assay Kit, 71285-3, LOT: 3728383
- Ripa: Sigma, R0278, LOT SLCD5849
- Protease: HaltTM Protease Inhibitor, Thermo Scientific, LOT WI334574
- NaF: Winkler, SO 1485
- Na3VO4: Sigma, S6508, LOT 14H087
- BSA for Protein quantification: Albumin Standard, Thermo Scientific, LOT UL289326
- Sodium chloride: Winkler, SO1455, LOT 14062016
- Potassium chloride: Winkler CAS 7447407, LOT 890000346386
- Sodium phosphate dibasic: Winkler SO1493, LOT 1418
- Potassium Phosphate monobasic: Winkler PO1290, LOT 724102
- Glycerol: Winkler, BM0800, LOT 20200449
- Mercaptoethanol: Winkler, BM1200, LOT N1564090
- Ponzu red: Winkler BM1492, LOT 91719
- Bromphenol Blue: Winkler, AZ0395, LOT71718
- Restore Plus Western Blot Stripping solution: Thermo Scientific, 46430, LOT VF297244.
- Digralasky Spreader: L-shape, EDLAB, LOT 202008
- Image J 1.53t, Wayne Rasband and contributors National Institute of Health, USA, http://imagej.nih.gov/ij
- GraphPad Prism 8 for Windows, Version 8.0.2 (263), https://www.graphpad.com/

8.3.2 Cell culture

- Cell culture plates: 6-wells, 24-wells, 96-wells, 60mm, 100mm: Costar – Corning Incorporated, REF: 3516, 3526, 3590, 14831, 430167
- DMEM low glucose: D5546, Sigma
- FBS - fetal bovine serum: F7524, Sigma
- Glutamine: G7513; Sigma
- Antibiotics/antimycotic: A5955; Sigma
- Cells: ECACC (European Collection of Authenticated Cell cultures), 94030304, LOT: 22A003
- All-trans-Retinoic acid (RA): R2625, Sigma
- Trypsin: Sigma, T4124
- Lithiumchlorid: Sigma-Aldrich, L9650-500G, Cas 7447-41-8, LOT BCCB9625
- Filter: EDLAB 305054233 or 280670892
- Microscope: Leica DMi8

8.3.3 Mice treatments

- Isoflurane: Baxter, Product-No: 218-082
- Chow: Prolab, RMH3000

8.3.4 Immunofluorescence

- Mounting medium: Fluromount-GTM, Electron Microscopy Sciences, 17984-25, LOT 210915
- Slides: EDLAB, CAT:7101
- PFA: Winkler, 011510, LOT: S5795215903
- Triton X-100: Winkler, BM2020, LOT M9218180
- Microscope: Leica DM2000 LED
- Lamp: Leica Kübler CODIX
- Camera: Mshot MDX6-T
- Imaging software: Mshot Image Analysis system v 1.0 Copyright 2014
- ImageJ-Fiji: 1.53t, Wayne Rasband and contributors National Institute of Health, USA, http://imagej.nih.gov/ij, Java 1.8.0_322 (64bit)
- Nail polish: Vogue fantastic

8.3.5 Antibodies

Table 5: Primary Antibodies
All used primary antibodies, origin and concentration. IF stands for Immunofluorescence

Target	Host	Con-centra-tion	Number and Company	Function	Size
Actin	Goat	1:000	Santa Cruz, sc-1616, LOT K0113	Housekeeping	42KD

ATF5	Mouse	1:000 or 1:100 (IF)	Santa Cruz, sc-377168, LOT I1522	mtUPR gene	35-55KD
Axin 2	Rabbit	1:000	Abcam, ab107613, LOT GR185092-3	WNT target gene	90KD
β-catenin	Mouse	1:000 or 1:200 (IF)	Santa Cruz, sc-7963, LOT C1313	WNT pathway	90KD
CamK *IV*	Rabbit	1:000	Abcam, ab3557	WNT target gene	55-70KD
ClpP	Mouse	1:000	Santa Cruz, sc-271284, LOT B0818	mtUPR gene	25KD
Dopamine receptor (D2DR)	Mouse	1:000	Santa Cruz, sc-5303, LOT D1717	Dopaminergic marker	~50KD
Dopamine transporter	Rat	1:000	Santa Cruz, sc-32259, LOT F2816	Dopaminergic marker	70KD
GADPH	Rat	1:000	Bio Legend, B289160, LOT G07902	housekeeping	35KD
GSK3β	Mouse	1:000	Santa Cruz, sc-377213	WNT pathway	50KD
Hsp60	Mouse	1:000	Thermo Fischer, MA3-012	mtUPR gene	60KD
LONP1	Rabbit	1:000	Invitrogen, PA5-51692, LOT YB3826223	mtUPR gene	100KD
MAP2	Mouse	1:000	Santa Cruz, sc-20172, LOT F2515	Dendritic marker	280KD
OMA1	Mouse	1:000	Santa Cruz, sc-515788, LOT 10922	mtUPR gene	40KD

pGSK3 (S9)	Rabbit	1:000	Santa Cruz, sc-81494, LOT J3111	inhibitory GSK3β	50KD
PSD95	Mouse	1:000	Santa Cruz, sc-32290	WNT target gene	95KD
Synaptophysin	Mouse	1:000	Santa Cruz, sc-17750, LOT 12617	Synaptic marker	35KD
Tau	Rabbit	1:000	Santa Cruz, sc-5587	Axonal marker	55KD
TOM20	Rabbit	1:000 or 1:100 (IF)	Santa Cruz, sc-11415, LOT C0614	mitochondrial marker	20KD
Tyrosine hydrox-ylase	Rabbit	1:000	Santa Cruz, sc-14007, LOT E0514	Dopaminergic marker	280KD
VDAC	mouse	1:000	Santa Cruz, sc-390996, LOT I2221	mitochondrial marker	40KD
β-tubulin	rabbit	1:000	Santa Cruz, sc-9104, LOT L1106	Housekeeping	55KD
Hsp70	goat	1:000	Santa Cruz, sc-1060, LOT G129	Housekeeping	70KD

Table 6: Secondary Antibodies
All used secondary antibodies, origin and concentration.

Secondary	Host	Concentration	Number and Company
Anti-mouse	G	1:5000	Jackson Im-muno Rese-arch, 115-035-003, LOT 158670
Anti-rat	G	1:5000	Jackson Im-muno Rese-arch, 112-005-003
Anti-rabbit	G	1:5000	Jackson Im-muno Rese-arch, 111-035-003, LOT 158675

Anti-goat	D	1:5000	Jackson Immuno Research, 705-035-003, LOT 154960
anti-mouse (Red Immunofluorescence)	G	1:200 (β-catenin), 1:100 (ATF5)	Invitrogen, Alexa fluro 555, A21422, LOT 1180091
anti-rabbit (green Immunofluorescence)	D	1:100	invitogen, Alexa fluro 488, A21206, LOT 215621

8.4 Python source code for Immunofluorescence analysis

8.4.1 Creation of merged images

```
# -*- coding: utf-8 -*-
"""
Created on Sun Aug 20 14:15:35 2023

@author: veronika
"""

import cv2
import numpy as np

#Ask for input names for red, green and blue
print ('Input name for red, If one of the following colours is not used input 0')
r = input()
print ('Input name for green')
g = input()
print ('Input name for blue')
b = input()
#Ask for the number of the pictures to be merged
print ('input the number of your first picture)
start = int(input())
print ('input the number of pictures +1')
num = int(input())
#Ask for the name to be saved
print ('input the name how you want it to be saved')
name = input()

for X in range(start, num): #From here on, the code goes through every picture in between the numbers we entered
    X = str(X)
```

```
    #To be able to use the number for opening the file, we need to change it to a string
    if r != 0: # check if the picture in this colour is available
        #read image
        red = r + X +'.tif'
        src_red = cv2.imread(red, cv2.IMREAD_UNCHANGED)
        # extract red channel -> [row, column, colour (blue = 0, green = 1, red = 2)] (:=alle)
        channel_red = src_red[:,:,2]
        # create an empty image with the same shape as that of your image
        merged_image = np.zeros(src_red.shape)
        #assign the red channel of src to the empty image
        merged_image[:,:,2]= channel_red
    # repeat the above code for green
    if g != 0:
        #read image
        green = g + X +'.tif'
        src_green = cv2.imread(green, cv2.IMREAD_UNCHANGED)
        print(src_green.shape)
        channel_green = src_green[:,:,1]
        # In case there is no red channel, we need to create a new image with  the same
        shape here
        if r == 0:
        merged_image = np.zeros(src_green.shape)
        merged_image[:,:,1]= channel_green
# repeat the above code for blue
if b != 0:
    blue = b + X +'.tif'
    src_blue = cv2.imread(blue, cv2.IMREAD_UNCHANGED)
    print(src_blue.shape)
    channel_blue = src_blue[:,:,0]
    if r == 0 and g == 0:
    merged_image = np.zeros(src_blue.shape)
    merged_image[:,:,0]= channel_blue
#save image
cv2.imwrite(name + X + '_python' + '.jpeg' ,merged_image)
```

8.4.2 Analysis of intensity in and out of the nucleus

```
import cv2
import numpy as np
import os.path
import locale

#Inform the user about the format of the pictures and the information needed for the
program
print('Please control all your picture names and change if necessary to the below format
in tif.\n Number of treatment_name of protein in colour X_number of picture_number of
cell.tif -> explanation: I treated cells with Lithium 0, 5 and 10mM --> 0mM = 1, 5mM = 2,
10mM = 3, I have atf5 for red, tom 20 for green and Hoesch for blue Example: 1_atf5_7_6
--> treatment 0mM, red channel, picture 7, cell 6')
# ask for the protein which needs to be in the name to differentiate the channel
```

```
print ('Input name of protein in primary channel')
print ('The primary channel is the channel of which the intensity is used to calculate. The overlapping channel is just telling you how much of your primary is in a certain compartment. the rest is given to you as a cell and tells you how much is outside of the compartment.')
r = input()
print ('Input name of protein in overlapping channel')
b = input()
print ('Which colour has your primary channel? (Blue = 0, Green = 1, Red = 2)')
channel_primary = int(input())
print ('Which colour has your overlapping channel? (Blue = 0, Green = 1, Red = 2)')
channel_overlap = int(input())
print ('please define your threshold by entering the lowest number x, the higher border is 255')
threshold = int(input())

# ask how many different treatments the person has to rotate through them
print ('input the number of treatments)
treatments = int(input())
# Define an empty list that the user fills with the first and last number of the pictures for every treatment and the first and last cell number of every picture. Needed to rotate through all the pictures and cells
start = []
finish = []
first =[]
last = []
# Have an error variable to tell the user in the end if something went wrong
error = 0

# first rotation through all the treatments
for treats in range (1, treatments+1):
    # ask for the first and last numbers of pictures for each treatment --> Information is saved in the opened lists
    print ('please enter your first picture of the treatment:', treats)
    start.append(int(input()))
    print ('please enter your last picture of the treatment:', treats)
    finish.append(int(input()))
    #now rotating through all pictures and asking for the first and last cell --> again stored in the opened lists
    for picture in range (start[treats-1],finish[treats-1]+1):
        print ('enter the first number of your cell in picture', picture)
        first.append(int(input()))
        print ('enter the last number of your cell in picture', picture)
        last.append(int(input()))
# The user is asked to name the file where all results are saved.
print ('enter the name of your Excel result file')
results = input()

#the file for the results is opened as an appending file, and an iteration variable is defined
```

```
i = 0
resultfile = open (results + '.csv', 'a')

# Rotations for calculating the results. It takes a treatment in the range of the treatments
given by the user
for T in range (1, treatments+1):
    # Then it takes the number for the first picture out of the list to the position of the
    treatment
    for X in range(start[T-1],finish[T-1]+1):
        #define an array to save all results so that they can then be written into the CSV
        resultarray2D = []
        resultarray2D.append(['Treatment ' + str(T) + '_picture' + str(X), 'Area', 'Mean',
        'IntDen'])
        Sum_allbackground = 0
      #Now rotate through all cells. Therefore, we need the iteration variable --> we take
      the value at the position 0 for the first picture. After the calculation, we increase i
      for one to take the new cell numbers for the next picture
      for Y in range (first[i], last[i]+1):
          #define needed variables
          Area_nucleus = 0
          IntDen_nucleus = 0
          Area_cell = 0
          IntDen_cell = 0
          Area_back = 0
          IntDen_back = 0
          Area_background = 0
          IntDen_background = 0
          CTCF = 0

          #read the image in red
          red = str(T)+ '_' + r + '_' + str(X) +'_'+ str(Y) +'.tif'
          #check if the picture exists. If not, go to the next picture
          if os.path.exists(red):
                src_red = cv2.imread(red, cv2.IMREAD_UNCHANGED)
                # extract red channel -> [row, column, colour] (:=all)
                channel_red = src_red[:,:,channel_primary]
                # create an empty image with the same shape as that of the src image
                src_pic = np.zeros(src_red.shape)
                #assign the red channel of src to the empty image
                src_pic[:,:,channel_primary]= channel_red
          #read the picture in blue
          blue = str(T) + '_' + b + '_' + str(X) +'_'+ str(Y) +'.tif'
          # check if the blue picture exists, then repeat the code of red for the blue
          if os.path.exists(blue):
                src_blue = cv2.imread(blue, cv2.IMREAD_UNCHANGED)
                channel_blue = src_blue[:,:,channel_overlap]
                src_pic[:,:,channel_overlap]= channel_blue
```

```
    #rotate through every single pixel in the picture by rotating through every
    value in the array.
    for x_value in range (0, src_pic.shape[0]):
        for y_value in range (0, src_pic.shape[1]):
        #check if the pixel in the wanted colour is greater than your threshold
        if src_pic[x_value,y_value,channel_primary] > threshold:
            #check both colours to find the overlapping areas. If both colours
            are over the threshold, add them to the nucleus group
            if src_pic[x_value,y_value,channel_overlap] > threshold:
                Area_nucleus = Area_nucleus + 1
                IntDen_nucleus = IntDen_nucleus +
                (src_pic[x_value,y_value,2]/3)
                #if only the first channel is over the threshold, add to the group
                cell
                else:
                    Area_cell = Area_cell + 1
                    IntDen_cell = IntDen_cell + (src_pic[x_value,y_value,2]/3)
                #If no pixel is over the threshold, add it to the background
                group.
                # The function calculates the Area = Number of pixels and Inte-
                grated density, which is the sum of all grey values
                # Grey values are the sum of all Intesnitys of a pixel in all col-
                ours (RBG) divided by 3
            else:
                Area_back = Area_back + 1
                IntDen_back = IntDen_back + (src_pic[x_value,y_value,2]/3)
        # The mean grey value is the Integrated density divided by the area ->
        calculated for all three groups of the above
        Mean_nucleus = IntDen_nucleus / Area_nucleus
        Mean_cell = IntDen_cell/Area_cell
        Mean_back = IntDen_back/Area_back
        # To calculate the mean grey value of all mean grey values of the back-
        ground, we sum up all of these means to use laterSum_allbackground
        = Sum_allbackground+Mean_back

        # The results are saved to the array to write into a CSV later
        resultarray2D.append(['Nucleus '+ str(Y), Area_nucleus, Mean_nu-
        cleus, IntDen_nucleus])
        resultarray2D.append(['Cell '+ str(Y), Area_cell, Mean_cell,
        IntDen_cell])
        resultarray2D.append(['Background '+ str(Y), Area_back, Mean_back,
        IntDen_back])
        #control and error message
        print(Mean_back, Mean_nucleus, Mean_cell)
        print ('cell ', Y,' of the picture ', X, ' was calculated')
    else:
        print('The blue picture ', blue, ' could not be found.')
        error += 1
else:
```

```
            print('The red picture', red, ' could not be found)
            error += 1

# The  red picture of the background is opened and again checked if it exists and see
the picture red
red = str(T)+ '_' + r + '_' + str(X) +'_b' +'.tif'
if os.path.exists(red):
    src_red = cv2.imread(red, cv2.IMREAD_UNCHANGED)
    # Extract red channel -> [zeile, spalte, Farbe] (:=alle)
    channel_red = src_red[:,:,channel_primary]
    # Create an empty image with the same shape as that of the src image
    src_background = np.zeros(src_red.shape)
    #assign the red channel of src to the empty image
    src_background[:,:,channel_primary]= channel_red

    # Repeat for the blue background picture
    blue = str(T)+ '_' + r + '_' + str(X) +'_b' +'.tif'
    if os.path.exists(blue):
        src_blue = cv2.imread(blue, cv2.IMREAD_UNCHANGED)
        channel_blue = src_blue[:,:,channel_overlap]
        src_background[:,:,channel_overlap]= channel_blue

        # All pixel intensities are added to the background group since no cells are in
        this picture
        for x_value in range (0,src_background.shape[0]):
            for y_value in range (0, src_background.shape[1]):
            # Again, Area, integrated density and mean are calculated
            Area_background = Area_background + 1
            IntDen_background = IntDen_background + (src_back-
            ground[x_value,y_value,2]/3)
        Mean_background = IntDen_background/Area_background
        Sum_allbackground = Sum_allbackground + Mean_background
        #mean of all backgrounds is calculated by dividing the sum by the number of
        analysed cells + background
        Mean_allbackground = Sum_allbackground/(last[i]+1)
        #again added to array to save
        resultarray2D.append(['background '+ str(X), Area_background, Mean_back-
        ground, IntDen_background])
        resultarray2D.append(['Mean_of_all_backgrounds '+ str(X), '', Mean_allback-
        ground, ''])
        #control message
        print ('picture ', X , ' is done')

        # rotating through all results in the array to find all results for cells and nu-
        cleus -> calculate the CTCF (Correlated Total Cell Fluorescence)
        for A in resultarray2D:
            if 'Nucleus' in A[0]:
                CTCF = A[3] - (A[1]* Mean_allbackground)
            elif 'Cell' in A[0]:
```

```
                    CTCF = A[3] - (A[1]* Mean_allbackground)
                else:
                    CTCF = ''
                # All results of the array and CTCF values are written in a CSV file to
                open later in Excel
                if 'de_' in locale.getlocale():
                    resultfile.write(str(A[0]).replace('.',',')+';'+str(A[1]).replace('.',',')+';'+
                    str(A[2]).replace('.',',')+';'+ str(A[3]).replace('.',',')+';'+ str(CTCF).re-
                    place('.',',')+ '\n')
                else:
                      resultfile.write(str(A[0])+';'+str(A[1])+';'+ str(A[2])+';'+ str(A[3])+';'+
                      str(CTCF)+ '\n')
            resultfile.write('\n')
            #control message
            print('results are written in excel')
            #increasing the iteration variable after all cells are calculated and before
            starting with the new picture.
            i += 1
        #error message
        else:
            print ('The blue background picture ', blue, ' could not be found.')
            error += 1
    else:
        print ('The red background picture ', red , ' could not be found.')
        error += 1

# Control and error message to summarise the errors for the user
if error == 0:
    print ('Program is done no errors occurred.')
else:
    print ('The program is finished with ', error, ' error messages.')

# close the resultfile
resultfile.close()
```